ANALYSIS OF VORTEX SHEDDING AROUND A CYLINDRICAL BODY IN A SUB-SONIC WIND TUNNEL

PROJECT REPORT

submitted by

VIMAL S V	132404001
KARTHIK R NARAYANAN	132414004
VIJAY P	132414005
ABHIRAM E R	132414006
RAKESH S S	132414011

UNDER THE GUIDANCE

of

Dr. T SUNDARARAJAN
Dr. PRAMOD KUNTIKANA

INDIAN INSTITUTE
OF TECHNOLOGY
PALAKKAD

Department of Mechanical Engineering

DECEMBER 2024

Course Project: *Analysis of vortex shedding around a cylindrical body in a Sub-sonic wind tunnel*

December 2024

ABSTRACT

This project involves the complete design and fabrication of a square cross-section wind tunnel, specifically engineered to create stable and controlled airflow conditions for experimental investigations. The primary focus is on analyzing vortex-shedding phenomena around cylindrical objects to better understand fluid flow behavior. A custom-built hot wire anemometer is employed utilizing a tungsten filament, allowing for precise and reliable data acquisition across different flow velocities. The experimental setup allowed measurements of airflow velocity under various conditions and facilitated the visualization of vortex-shedding using smoke, providing a clear view of the complex flow patterns. The data collected were used to establish the relationship between the Reynolds number (Re), which characterizes the flow regime, and the Strouhal number (St), which quantifies the frequency of vortex shedding. This analysis revealed significant insights into how variations in flow velocities influence vortex-shedding behavior and how these phenomena can be correlated with fundamental fluid dynamics principles. The findings contribute to a deeper understanding of fluid flow dynamics in controlled settings, serving as a foundational framework for future research focused on advanced sensing techniques and simulation models. This helps in further investigation and prediction of the behavior of complex fluid systems.

Keywords: Vortex shedding, Wind Tunnel, Flow visualization

ACKNOWLEDGMENTS

First and foremost, we would like to express our sincere gratitude to our advisors, Dr. T Sundararajan and Dr. Pramod Kuntikana for their guidance, patience, motivation, and continuous support during the course of our project and smooth completion of the course. We would also like to thank Indian Institute of Technology Palakkad for giving chance to do this course project as part of Measurements in Thermofluids course.

We would like to express sincere gratitude to all the teaching assistants and our co research scholars Mr. Ajith U K Nair, Mr. Arundas Odungat, Mr. Vaishak Rajendran Pillai, Mr. Ragupathi A P, Mr. Ubaidulla C T, Mr. Muruga Prabu U, special mention to Mr. Sabareesh V for their valuable support and guidance throughout semester for smooth completion of lab experiments and their valuable insights and discussions for completion of this course project.

We would like to thank other faculty members of Department of Mechanical Engineering special mention to Dr. Anoop Akkoorath Mana, Dr. Dinesh Setti, Dr. Kanmani Subbu, Dr. Ganesh Natarajan and Dr. Vineed Narayanan for their valuable support, guidance and their help at various stages of this project. We would also like to thank all the staffs of Mechanical Engineering especially Mr. Bharath Krishna and Mr. Ganesha for helping us at different stages of this project.

We would like to thank CSquare Innovation Lab of IIT Palakkad, Chief Innovation officer Dr. Jacob Chandapillai for providing facilities for fabrication of experimental setup. We would also like to thank staffs of CSquare Innovation lab, Mr. Pradeep and Mr. Vinod for their help during fabrication in lab.

Last but not the least, we would like to express our sincere gratitude to our family members for their unconditional love, support, motivation and encouragement. We would also like to thank the Almighty for smooth completion of our project.

CONTENTS

I Introduction, Literature review and Design

1 Introduction 3

1.1 Objectives: . . . 3

1.2 Organization of the report . . . 4

2 Literature review 5

3 Design and fabrication 7

3.1 Elements of the Wind Tunnel Setup: . . . 7

3.2 Main parts of the wind tunnel: . . . 8

3.2.1 Settling chamber . . . 8

3.2.2 Contraction Section . . . 9

3.2.3 Test Section . . . 10

3.2.4 Diffuser Section . . . 11

3.3 Hot Wire Filament . . . 12

3.4 Fan Power calculation . . . 13

3.4.1 Area Calculations . . . 13

3.4.2 Flow Rate Calculation . . . 13

3.4.3 Pressure Drop Calculations . . . 13

3.5 Design Summary of the wind tunnel . . . 16

II Procedure and results

4 Experimental procedure 19

4.1 Calibration of tungsten filament of the bulb . . . 19

4.2 Time constant of the filament of the bulb . . . 23

4.3 Calibration of Hot wire anemometer . . . 24

4.4 Time constant of the hot wire anemometer . . . 27

4.5 Chapter summary . . . 27

5 Results and discussions 29

5.1 Vortex analysis at distance $x = D$ from the cylinder . . . 29

5.1.1 Vortex analysis at the center of the cylinder . . . 29

5.1.2 Vortex analysis at a height of 0.5 D from the center of the cylinder 33

5.2 Vortex analysis at distance $x = 2D$ from the cylinder . . . 35

5.2.1 Vortex analysis at the center of the cylinder . . . 35

5.2.2 Vortex analysis at a height of 0.5 D from the center of the cylinder 37

5.3 Vortex analysis at distance x = 4D from the cylinder 39
5.3.1 Vortex analysis at the center of the cylinder 39
5.3.2 Vortex analysis at a height of 0.5 D from the center of the cylinder 41
5.4 Chapter summary 43

III Conclusion and future scope

6 Conclusions 47
6.1 Future scope 48

Bibliography 49

LIST OF FIGURES

Figure 3.1 Wind tunnel test rig. 8
Figure 3.2 Dimensions of converging section. 9
Figure 3.3 Dimensions of the test section. 10
Figure 3.4 Dimensions of diverging section. 11
Figure 4.1 Calibration of tungsten filament of the bulb 19
Figure 4.2 Voltage variation with time for a flow having pressure of 4 Pa recorded in a PC oscilloscope. 20
Figure 4.3 Comparison of measured voltage and Calculated voltage of the filament of a bulb. 22
Figure 4.4 Response of the tungsten filament of the bulb to the step input. 23
Figure 4.5 Calibration of hot wire anemometer. 24
Figure 4.6 Comparison of measured and calculated voltage of the hot wire anemometer 26
Figure 4.7 Response of a hot wire anemometer for a step input. 26
Figure 5.1 The variation of voltage with time for a flow having differential pressure of 1 Pa for sensor placed at a distance of D from the cylinder 29
Figure 5.2 The variation of velocity with time for a flow having differential pressure of 1 Pa for sensor placed at a distance of D from the cylinder 30
Figure 5.3 Frequency spectrum of velocity. 31
Figure 5.4 Frequency spectral density of velocity for flow Reynolds number (a) 2699, (b) 3818, (c) 4676 and (d) 5399 at a distance of D from the center of the cylinder. 32
Figure 5.5 Variation of Strouhal number (St) with Reynolds number (Re) for flow past a cylinder at a distance of "D" from the center. . . 33
Figure 5.6 Frequency spectral density of velocity for flow Reynolds number (a) 2699, (b) 3818, (c) 4676 and (d) 5399 at a distance of "D" and a height of "0.5 D" from the center of the cylinder. 34
Figure 5.7 Variation of Strouhal number (St) with Reynolds number (Re) for flow past a cylinder at a distance of "D" and at a height of "0.5 D" from the center of the cylinder. 35

Figure 5.8 Frequency spectral density of velocity for flow Reynolds number (a) 2699, (b) 3818, (c) 4676 and (d) 5399 at a distance of "2 D" from the center of the cylinder. 36
Figure 5.9 Variation of Strouhal number (St) with Reynolds number (Re) for flow past a cylinder at a distance of "2 D" from the center of the cylinder. 37
Figure 5.10 Frequency spectral density of velocity for flow Reynolds number (a) 2699, (b) 3818, (c) 4676 and (d) 5399 at a distance of "2 D" and a height of "0.5 D" from the center of the cylinder. 38
Figure 5.11 Variation of Strouhal number (St) with Reynolds number (Re) for flow past a cylinder at a distance of "2 D" and at a height of "0.5 D" from the center of the cylinder. 39
Figure 5.12 Frequency spectral density of velocity for flow Reynolds number (a) 2699, (b) 3818, (c) 4676 and (d) 5399 at a distance of "4 D" from the center of the cylinder. 40
Figure 5.13 Variation of Strouhal number (St) with Reynolds number (Re) for flow past a cylinder at a distance of "4 D" from the center of the cylinder. 41
Figure 5.14 Frequency spectral density of velocity for flow Reynolds number (a) 2699, (b) 3818, (c) 4676 and (d) 5399 at a distance of "4 D" and a height of "0.5 D" from the center of the cylinder. 42
Figure 5.15 Variation of Strouhal number (St) with Reynolds number (Re) for flow past a cylinder at a distance of "4 D" and a height of "0.5 D" from the center of the cylinder. 43

LIST OF TABLES

Table 3.1 Design summary of wind tunnel. 16
Table 4.1 The flow velocity and the output mean voltage of the tungsten filament of the bulb. 21
Table 4.2 The difference of calibrated voltage from measured voltage for filament of the bulb. 22
Table 4.3 The flow velocity and the output mean voltage of the hot wire anemometer. 25

Table 4.4 The difference of calibrated voltage from measured voltage for hot wire anemometer. 25

Part I

INTRODUCTION, LITERATURE REVIEW AND DESIGN

1

INTRODUCTION

The study of fluid flow around bluff bodies, such as cylindrical structures, is an essential aspect of engineering and scientific research due to its widespread implications in both natural and industrial contexts. One key phenomenon in this field is vortex shedding, where alternating vortices are generated in the wake of a cylindrical object as fluid flows over it. This effect can result in periodic forces acting on the structures, which can cause vibrations that affect their stability, lifespan, and performance. Such vortex-induced vibrations are particularly significant for applications involving bridges, tall buildings, towers, pipelines, and offshore structures. Understanding the conditions under which vortex shedding occurs and how it behaves is crucial for designing structures that can withstand these dynamic forces without failure. To explore this phenomenon in a controlled environment, this project focuses on the design, fabrication, and testing of a wind tunnel tailored for investigating vortex shedding around cylindrical objects. The wind tunnel is designed to facilitate consistent airflow conditions for various Reynolds numbers, thus enabling the study of changes in flow velocity which affects the vortex shedding process. In addition, a constant current hotwire anemometer is utilized to accurately measure vortex shedding frequencies, while smoke visualization is used for qualitative analysis of vortex formation and behavior. This project aims to connect experimental observations with theoretical concepts, enhancing the understanding of vortex shedding and contributing to advances in fluid mechanics research.

1.1 OBJECTIVES:

1. Design a square cross-section wind tunnel capable of generating controlled airflow over a cylindrical test object, ensuring steady flow conditions.
2. Visualize vortex shedding and flow patterns around the cylindrical test object using smoke.
3. Measure airflow velocity and hence vortex shedding frequency using a hot wire anemometer and tungsten bulb filament, ensuring accurate data capture in turbulent flow regime.

4. Compare velocity data from both measurement techniques to assess their consistency, accuracy, and reliability under varying velocity flow conditions.
5. Analyze the relationship between flow velocity, vortex formation, and flow characteristics (e.g., turbulence) around the test object.
6. Analyze the results and plot St (Strouhal number) versus Re (Reynolds number) to understand the behavior of vortex shedding at various flow conditions.

1.2 ORGANIZATION OF THE REPORT

This project report has three parts.

- Part I contains the introduction and the literature review chapters.
- Part II includes Chapters 3, 4 and 5:
  - Chapter 3 discusses the design parameters of the wind tunnel - size and shape of convergent, divergent and test sections. It also discusses the design of the hot wire anemometer
  - Chapter 4 discusses calibration procedure of both the tungsten filament of the bulb and the hot wire anemometer. The chapter also discusses the time constant and the selection of sensor for this project.
  - Chapter 5 discusses the behavior of vortex in the wind tunnel at different locations. In addition, it discusses the relation between the Reynolds number and the Strouhal number at those locations
- Part III briefs the conclusions on the work presented in this report.

2

LITERATURE REVIEW

The study by Doolan *et al*. [1] focuses on the behavior of vortex shedding in the wake of a cylinder subjected to flow through a gap, with a particular emphasis on how the gap-to-diameter ratio (denoted as G/D) influences the spectral properties of the wake. The paper provides valuable insights into the interaction between shear layers and the formation of quasi-stable vortices in the near wake, a critical phenomenon in fluid dynamics, particularly in the context of flow-induced vibrations, aero acoustics, and the design of cylindrical structures in flow environments.

Hauptmann *et al*. [2] developed an affordable and robust hot wire anemometer using a filament from a flashlight bulb, which makes it suitable for educational and practical applications despite a slight reduction in precision due to filament looping. This design addressed the fragility and high cost of traditional tungsten or platinum probes, allowing for a wider use in turbulence and fluid flow studies. Similarly, Griffith *et al*. [3] and Singha and Sinhamahapatra (2010) observed an increase in St with confinement, although Turki et al. (2003) noted a decreasing trend. For vertical confinement (h), studies such as Inoue and Sakuragi (2008) reported an increase in both St and critical Re as h decreased.

Ishan J. Kelkar *et al.*. [4]. This article incorporates a discussion on arranging and gathering an unassuming wind current that can be utilized for instructive purposes. The objective was to make a satisfactory wind stream at a speed of 10 m/s in the test fragment and to incorporate factors like traditionalism, comfort, and robustness into the development. Another objective was to direct an investigation on comparable proliferation and show the differentiation among numerical and exploratory outcomes.

Amol L. Mangrulkar *et al.*. [5] discuss the design and assembly of a simple wind tunnel suitable for educational purposes. The goal was to achieve adequate airflow with a speed exceeding 10 m/s in the test section, incorporating factors such as simplicity, comfort, and durability in its construction. Another objective was to conduct an investigation on vortex shedding and compare the results between numerical simulations and experimental data.

3D experimental studies by Rehimi *et al.* [6] and Jung *et al*. (2012) extended the analysis to confined 3D flows, identifying trends in recirculation length and wake dynamics, while time-resolved data capturing transient vortex-shedding in microscale flows remain scarce due to the limitations of conventional micro PIV systems.

Sahin and Owens [7] demonstrated that increasing lateral confinement (reducing w) raises the critical Re for vortex-shedding. 2D simulations of lateral confinement, as studied by Singha and Sinhamahapatra . [8], provided valuable insight into the trends of vortex-shedding frequency.

3

DESIGN AND FABRICATION

In this chapter, the elements of wind tunnel, the design dimensions and its calculations with respect to the solid cylinder are discussed.

3.1 ELEMENTS OF THE WIND TUNNEL SETUP:

1. Test Section: In the test section, a solid cylinder is placed at the center to induce vortex shedding. As air flows past the cylinder, it generates a turbulent wake leading to vortex formations, which needs to be studied to understand the dynamics of fluid flow and the effects of varying conditions such as flow velocity (Reynolds number).

2. Flow Control (Exhaust Fan or Suction Fan): The air flow through the wind tunnel is generated by an exhaust fan that creates a continuous flow of air. This suction fan is integrated into the system to help maintain a consistent air velocity by drawing air through the tunnel, ensuring steady and controlled flow conditions for the experiments.

3. Hot-Wire Anemometer: The hot wire anemometer in this set-up is directly connected to a constant current DC source and an oscilloscope. The DC source provides a steady current to the hot wire, which heats up as the current passes through it. As air passes through the wire, it cools the wire, causing a change in its electrical resistance. These changes in resistance are captured by the oscilloscope, allowing real-time monitoring of the airflow velocity. The oscilloscope displays the voltage fluctuations, which correspond to variations in airspeed, providing detailed data for analyzing vortex-shedding behavior and other characteristics of fluid dynamics.

The wind tunnel is designed with a square cross section, providing adequate space for the cylindrical test object and allowing air flow to develop uniformly before reaching the test section. The dimensions of the tunnel are chosen to ensure a stable and controlled environment for accurate experimentation.

3.2 MAIN PARTS OF THE WIND TUNNEL:

This section discusses the main parts of the wind tunnel. Each part serves a specific purpose, such as improving flow quality, controlling velocity, or ensuring stable air flow to and from the test section. Fig. 3.1 shows the basic wind tunnel test rig used in this project. There are certain assumptions made, which are given below:

Figure 3.1: Wind tunnel test rig.

- The air flows in the subsonic region and is incompressible.
- The tunnel is assumed to be steady, with a uniform flow before the cylinder.
- The Reynolds number will be chosen on the basis of typical flow conditions in the wind tunnel.

The following sections discuss the parts of the wind tunnel.

3.2.1 *Settling chamber*

The settling chamber is the first section of the wind tunnel. Its primary purpose is to stabilize the air flow and remove large turbulence before the air moves into the contraction section.

3.2.1.1 *Length calculations:*

The length of the settling chamber is usually between 0.25 to 4 times the width of the tunnel. Width of the settling chamber ($W_{settling}$) is taken as 0.4 m. The length of the settling chamber ($L_{settling}$) should be between 0.1 m and 0.15 m and it is taken as 0.1 m for better flow conditioning.

3.2.2 *Contraction Section*

The contraction section is used to accelerate the flow towards the test section while ensuring that the air flow remains smooth. This section converges the cross-sectional area, accelerating the air and increasing the velocity as it moves through the wind tunnel.

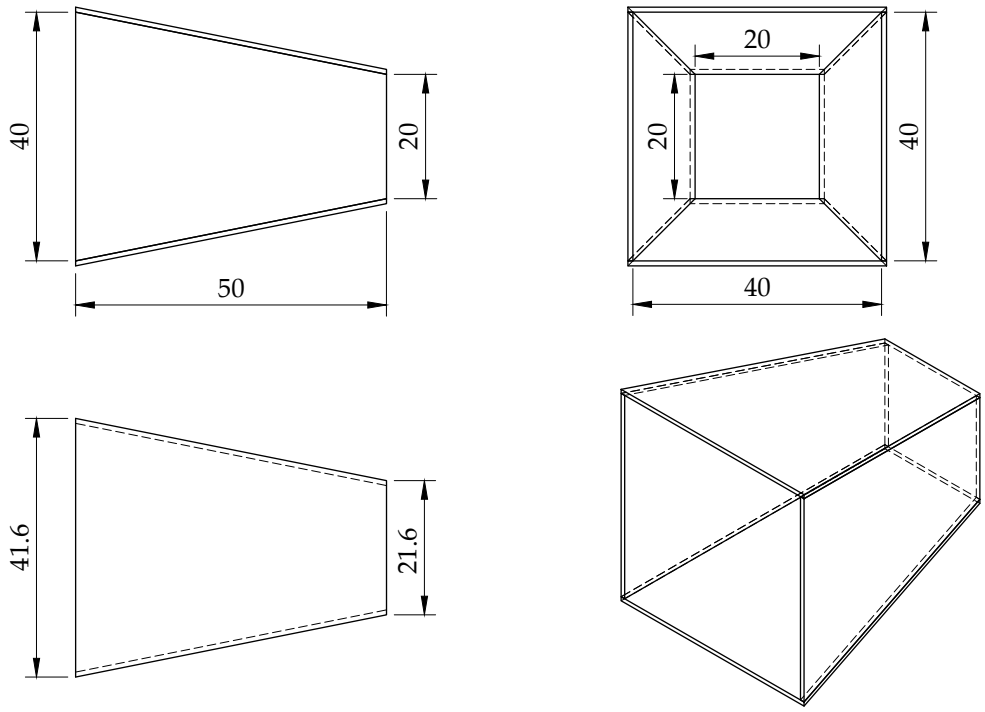

Figure 3.2: Dimensions of converging section.

3.2.2.1 *Design Parameters*

A typical contraction ratio (the ratio between the cross-sectional area of the inlet and the cross-sectional area of the test section) is 4:1 for laminar flow. This ensures that the air accelerates smoothly as it enters the test section. The height of the contraction section, $H_{Contraction}$ = 20 cm and the width of the contraction section, $W_{Contraction}$ = 20 cm. The length of the contraction section is typically 2 to 5 times the width of the test section. So, length of the contraction section, $L_{Contraction}$ = 0.5 m

3.2.3 *Test Section*

The object (solid cylinder) is placed in the test section and the vortex shedding and flow measurements are analyzed. The air flow for analysis should be uniform. The test section provides uniform airflow for analysis. The calibration of the bulb filament and the hot wire anemometer is performed in the test section. Vortex analysis is also performed in the test section.

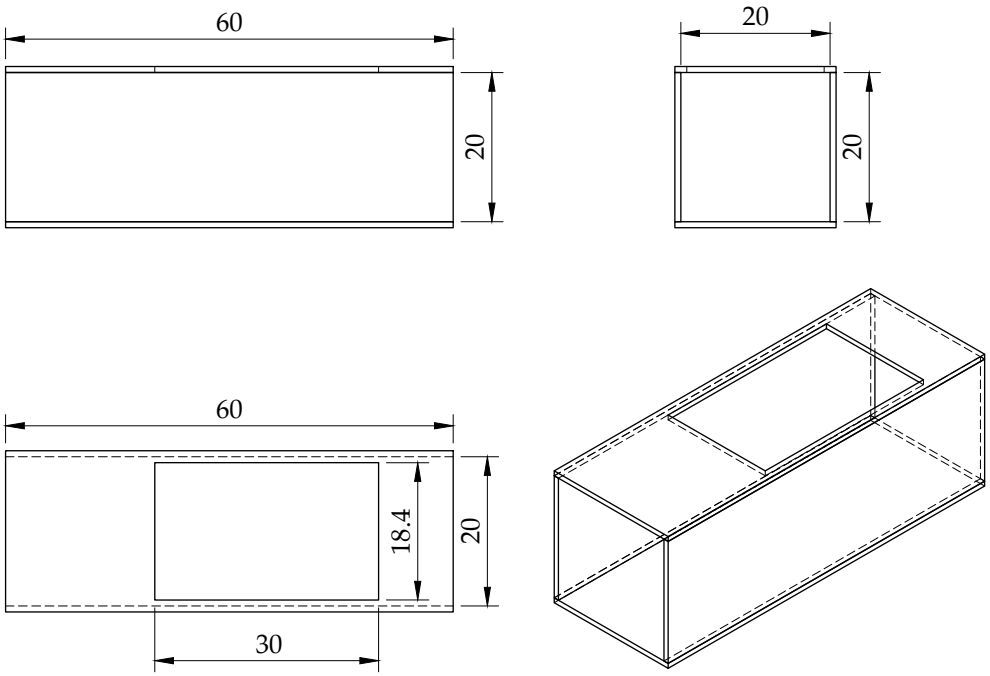

Figure 3.3: Dimensions of the test section.

3.2.3.1 *Design parameters:*

The width and height of the test section should be at least 5–10 times the diameter of the cylinder. The diameter of the D-cylinder is 0.033 m (33 mm). So width and height of the test section is

$$W_{test} = 7 \times D = 7 \times \ 0.033 = 0.23m, \tag{3.1}$$

$$H_{test} = 7 \times D = 7 \times 0.033 = 0.23m. \tag{3.2}$$

So, the test section is designed to have a square cross section of side having 20 cm length. The length of the test section should be long enough to allow a fully developed flow before the air flow reaches the cylinder. The length is typically between 10 to 20

times the diameter of the test object (the cylinder) to allow for stable flow development. So, the length of the test section,

$$L_{test} = 18 \times D = 18 \times 0.033 = 0.6m \tag{3.3}$$

3.2.4 *Diffuser Section*

The Diffuser Section is the final section of the wind tunnel, and its purpose is to slow down the airflow after the test section while minimizing turbulence. In this section, the airflow expands in the cross-sectional area, leading to a decrease in the velocity of the air, which helps to prevent any damage or instability in downstream equipment such as fans or flow measurement instruments. In addition, the diffuser allows the pressure to recover smoothly. The diffuser should have a gentle expansion to avoid turbulent separation. The cross-sectional area of the diffuser gradually increases, which reduces the velocity of the flow. The expansion ratio (the ratio of the inlet to the outlet area) is typically between 1.5:1 to 2:1 to ensure smooth deceleration without flow separation.

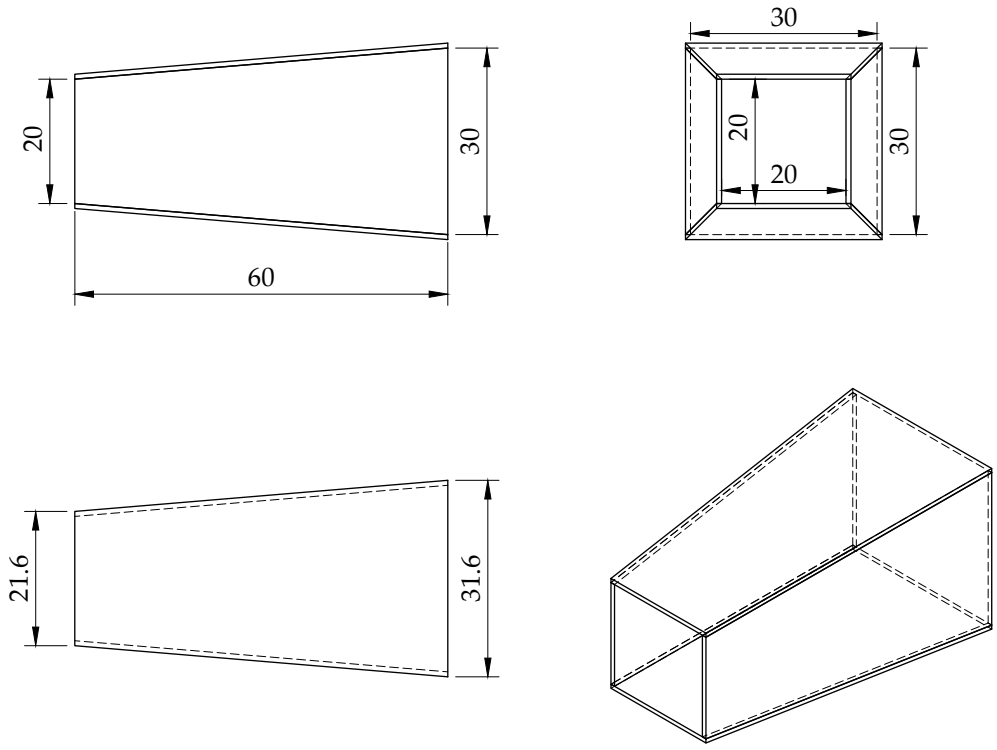

Figure 3.4: Dimensions of diverging section.

3.2.4.1 *Design parameters*

The diffuser must also allow for the transition from the uniform flow of the test section to the slower flow at the exit of the tunnel. The cross section of the diffuser section near the test section should be equal to the cross section of the test section. It should gradually increase at the other end for smooth flow expansion. So, the width ($W_{diffuser}$) and height ($H_{diffuser}$) of the diffuser near the test section is 0.2 m and it is 0.4 m at the end.

Length of the diffuser should be long enough to allow the flow to gradually decelerate and the pressure to recover smoothly. The length is generally 2 to 5 times the width of the diffuser section. Since the diffuser width at the end is 0.3 m, the length of the diffuser is

$$L_{Diffuser} = 2 \times 0.3 = 0.6 \text{ m}$$

To design a gentle expansion, the ratio of the inlet area (of the test section) to the outlet area (of the diffuser) should be between 1.5:1 to 2:1. This would allow the air to decelerate without excessive turbulence.

3.3 HOT WIRE FILAMENT

When selecting a hot wire filament that is used in light bulbs or heating elements, it is essential to calculate its resistance, surface area and the maximum temperature at which the filament can operate safely. Below is a detailed breakdown of how to select the filament based on the provided information: The resistance of the filament and the operating temperature are calculated on the basis of material properties and filament dimensions. The resistance R of the filament can be estimated using the equation

$$R = \rho_w \frac{L_w}{A_w}, \tag{3.4}$$

where ρ_w is the resistivity of tungsten ($5.6 \times 10^{-8} \Omega m$), L_w is the length of the filament (4 mm) and A_w is the cross-sectional area of the filament (7.853×10^{-12} m^2). Substituting the values in Eq. (3.4), the resistance R of the filament is estimated to be 0.03Ω. The maximum operating temperature of the filament is determined using the energy balance equation

$$I^2 R = hA_w(T_{wire} - T), \tag{3.5}$$

where I is the current, R is the resistance of the wire (Eq. (3.4)), h is the heat transfer coefficient (10 W/m^2K), A is the surface area of the filament (1.256×10^{-5} m^2) and

T is the ambient temperature (32°C). Substituting the above values in Eq. (3.5), the maximum filament temperature T_{wire} can be estimated to be 300°C. Thus, the tungsten filament will operate at a maximum temperature of approximately 300 ° C.

3.4 FAN POWER CALCULATION

This section provides a detailed calculation to determine the required fan power for a wind tunnel with the dimensions described in the previous section and the flow conditions.

3.4.1 *Area Calculations*

Area of the contraction section

$$A_{contraction} = W_{contraction} \cdot H_{contraction} = 0.4 \cdot 0.4 = 0.16 \text{ m}^2, \tag{3.6}$$

area of the test section

$$A_{test} = W_{test} \cdot H_{test} = 0.2 \cdot 0.2 = 0.04 \text{ m}^2 \tag{3.7}$$

and the area of the diffuser section

$$A_{diffuser} = W_{diffuser} \cdot H_{diffuser} = 0.3 \cdot 0.3 = 0.09 \text{ m}^2. \tag{3.8}$$

3.4.2 *Flow Rate Calculation*

The air flow rate Q in the test section is calculated as

$$Q = A_{test} \cdot V_m = 0.04 \cdot 20 = 0.8 \text{ m}^3/\text{s}, \tag{3.9}$$

where A_{test} is the area of the test section (Eq. (3.7)) and V_m is the maximum air flow velocity which is assumed as 20 m/s.

3.4.3 *Pressure Drop Calculations*

The pressure drop in the settling chamber is given by

$$\Delta P_{settling} = k_{settling} \cdot \frac{\rho V_{settling}^2}{2}, \tag{3.10}$$

where $k_{settling}$ is the loss factor (= 1.5), ρ is the density of the air and $V_{settling}$ is the velocity of the air flow in the settling chamber. The air and settling chamber contact

area includes the straw area that is placed to obtain uniform air flow. The contact area is given by

$$A_{straws} = A_{contraction} \cdot \text{porosity factor} = 0.16 \cdot 0.8 = 0.128 \text{ m}^2. \tag{3.11}$$

From Eqs. (3.9) and (3.11), the velocity of the air at the settling chamber is

$$V_{settling} = \frac{Q}{A_{straws}} = \frac{0.8}{0.128} = 6.25 \text{m/s}. \tag{3.12}$$

Substituting Eq. (3.12) in Eq. (3.10), the pressure drop in the settling chamber is calculated as

$$\Delta P_{settling} = 1.5 \cdot \frac{1.21 \cdot 6.25^2}{2} = 35.16 \text{ Pa}. \tag{3.13}$$

The pressure drop in the contraction section is given by

$$\Delta P_{contraction} = k_{contraction} \cdot \frac{\rho V_m^2}{2}, \tag{3.14}$$

where $k_{contraction}$ is the loss factor (= 0.1), V_m is the maximum velocity of the air in the test section. Substituting all the values, the pressure drop in the contraction section is calculated as

$$\Delta P_{contraction} = 0.1 \cdot \frac{1.21 \cdot 20^2}{2} = 24 \text{ Pa}. \tag{3.15}$$

The pressure drop in the test section is given by

$$\Delta P_{test} = \frac{1}{2} \rho V_m^2 f_f \frac{L_{test}}{D_h}, \tag{3.16}$$

where f_f is the friction factor (= 0.02), L_{test} is the length of the test section (Eq. (3.3)) and D_h is the hydraulic diameter given by

$$D_h = \frac{4 \cdot A_{test}}{P_{test}}, \tag{3.17}$$

where A_{test} is the area of cross section of the test section (Eq. (3.7)). P_{test} is the wetted perimeter of the test section given by

$$P_{test} = 2 \cdot (W_{test} + H_{test}) = 2 \cdot (0.2 + 0.2) = 0.8 \text{ m}, \tag{3.18}$$

where W_{test} is the width of the test section (Eq. (3.1)) and H_{test} is the height of the test section (Eq. (3.2)). Substituting Eqs. (3.7) and (3.18) in Eq. (3.17), the hydraulic diameter of the test section is calculated as

$$D_h = \frac{4 \cdot 0.04}{0.8} = 0.2 \text{ m} \tag{3.19}$$

Substituting Eqs. (3.3), (3.19) in Eq. (3.16), the pressure drop in the test section is calculated as

$$\Delta P_{test} = \frac{1}{2}(1.21)(20)^2(0.02)\frac{0.6}{0.2} = 14.4 \text{ Pa} \tag{3.20}$$

The pressure drop in the diffuser section is given by

$$\Delta P_{diffuser} = k_{diffuser} \times \frac{\rho V_m^2}{2} = 0.2 \times \frac{1.21 \times 20^2}{2} = 48 \text{ Pa}, \tag{3.21}$$

where k_{diff} is the loss factor in the diffuser (= 0.2). From Eqs. (3.13), (3.15), (3.20) and (3.21), the total pressure drop in the wind tunnel is

$$\begin{aligned} \Delta P_{total} &= \Delta P_{settling} + \Delta P_{contraction} + \Delta P_{test} + \Delta P_{diffuser}, \\ \Delta P_{total} &= 35.16 + 24 + 2 + 48 = 109.16 \text{ Pa}. \end{aligned} \tag{3.22}$$

The required power of the suction fan can be calculated as

$$P_{fan} = \frac{\Delta P_{total} \cdot Q}{\eta}, \tag{3.23}$$

where ΔP_{total} is the total pressure drop in the wind tunnel (Eq. (3.22)), Q is the air flow rate in the wind tunnel (Eq. (3.9)) and η is the efficiency (= 0.7). Substituting above values, the power of the suction fan is calculated as

$$P_{fan} = \frac{109.16 \times 0.8}{0.7} = 124.7 \text{ W} \approx 0.167 \text{ HP}. \tag{3.24}$$

For an air flow velocity of 20 m/s, the required power of the suction fan is approximately 0.167 HP. In this project, the power of the suction fan used is 0.5 HP, which is sufficient to carry out this project.

3.5 DESIGN SUMMARY OF THE WIND TUNNEL

Table 3.1: Design summary of wind tunnel.

Section	Length (m)	Length (m)	Length (m)	Purpose
Settling chamber	0.1	0.4	0.4	To remove turbulence and stabilize the flow
Converging section	0.5	0.2	0.2	To accelerate the flow towards the test section
Test section	0.6	0.2	0.2	To perform testing with uniform flow around the cylinder
Diffusing section	0.6	0.3	0.3	To decelerate the flow after the test section
Fan (Suction type - Power 0.5 hp)	-	0.3	0.3	To house the fan and expel air from the system

The suction-type fan, with a power of 0.5 HP and dimensions of 0.3 m × 0.3 m, is designed to accommodate the fan mechanism and efficiently expel air from the system.

Part II

PROCEDURE AND RESULTS

4

EXPERIMENTAL PROCEDURE

In this chapter, the procedure for the experiment is discussed in detail. The experimental procedure starts with calibration of the measuring equipment using a known standard and further using the calibrated equipment to analyze the vortices in the flow.

4.1 CALIBRATION OF TUNGSTEN FILAMENT OF THE BULB

In this section, the calibration process of tungsten filament is discussed. First, the filament is kept at the middle of the test section and a constant current of 0.310 A is supplied to it (see Fig. 4.1). The output of the filament, which is the voltage variation, is recorded in a PC oscilloscope for a time of 5 s without any flow. This data corresponds to no flow condition. The suction fan is then kept at a low speed. The pressure difference in the flow due to the increased speed of the flow is measured using the standard pitot static tube. The corresponding voltage variation in the filament is measured in the PC oscilloscope. Further, the speed of the suction fan is increased and the output is taken both from the pitot static tube and the filament.

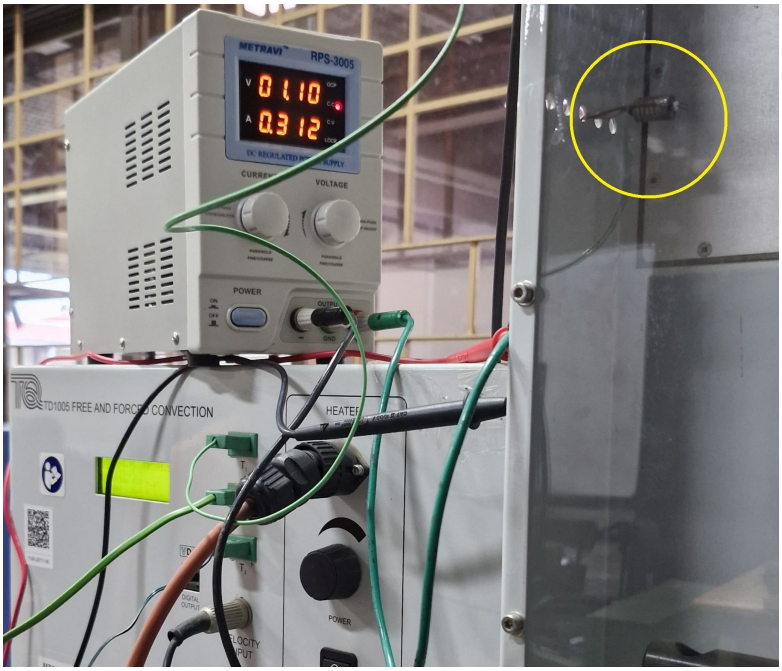

Figure 4.1: Calibration of tungsten filament of the bulb

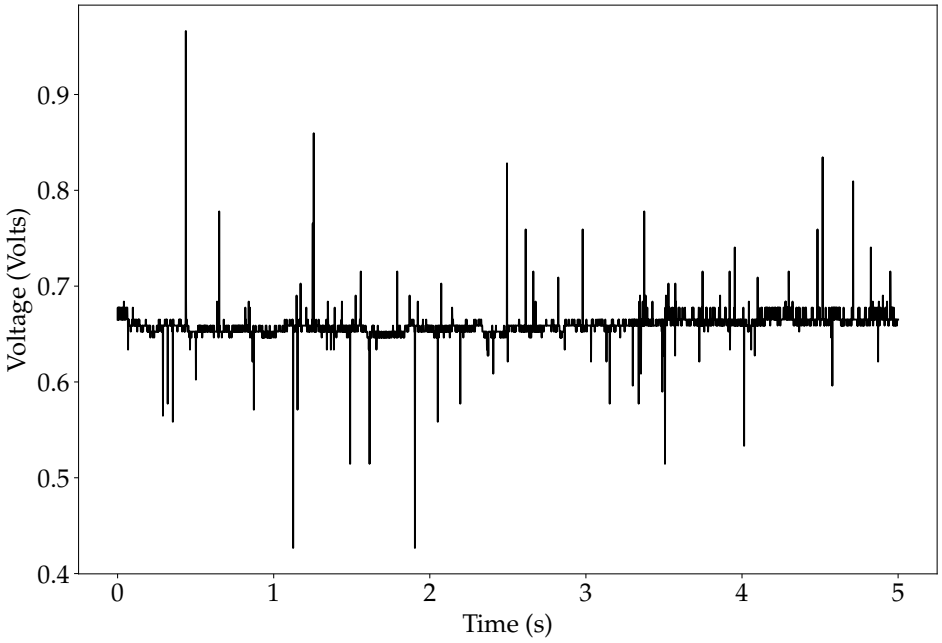

Figure 4.2: Voltage variation with time for a flow having pressure of 4 Pa recorded in a PC oscilloscope.

The output voltage of the filament measured from the oscilloscope for a pitot tube pressure of 4 Pa is given in Fig. 4.2. From the figure, it can be seen that there are fluctuations in the voltage. For calculation purposes, the mean value of the voltage fluctuation is considered. The same procedure is followed for other flow velocities. The filament output voltage is recorded for a pitot tube pressure of 1 Pa, 2 Pa, 3 Pa, 4 Pa, 6 Pa, 9 Pa, 12 Pa, 14 Pa, 17 Pa, 19 Pa and 24 Pa. The flow velocity corresponding to pitot static tube pressure is calculated using Eq. (4.1).

$$U = \sqrt{\frac{2\Delta P}{\rho}}, \tag{4.1}$$

where ΔP is the differential pressure measured in the pitot static tube and ρ is the density of air (= 1.21 kg/m^3). The differential pressure, velocity, and corresponding voltage output of the filament is given in Table 4.1. The tungsten filament is then calibrated by applying the output from the pitot tube into King's law,

$$E^2 = E_0^2 - BU^n, \tag{4.2}$$

where E is the measured mean output voltage, E_0 is the mean voltage corresponding to no flow condition, U is the flow velocity. B and n are numerical constants that can be estimated by regression analysis while calibrating the filament. Equation. (4.2) is

$$E_0 = 1.09\ V$$

Table 4.1: The flow velocity and the output mean voltage of the tungsten filament of the bulb.

Differential Pressure ΔP (Pa)	**Velocity U (m/s)**	**Mean Voltage E (Volts)**
1	1.307	0.842
2	1.849	0.756
3	2.265	0.689
4	2.615	0.659
6	3.203	0.641
9	3.922	0.653
12	4.529	0.621
14	4.892	0.596
17	5.391	0.642
19	5.699	0.599
24	6.405	0.561

an exponential function that can be linearized by taking logarithms. Rearranging and taking natural log on both sides of Eq. (4.2) gives

$$\ln (E_0^2 - E^2) = n \ln U + \ln B. \tag{4.3}$$

Equation (4.3) is the linearized form of King's law and can be expressed in the form $y = mx + c$. The linearized King's law equation can be solved using the method of least squares to find the numerical constants B and n. The solution steps for method of least squares is given by

$$\Sigma \ln (E_0^2 - E^2) = n\Sigma \ln U + q \ln B \tag{4.4}$$

$$\Sigma(\ln (E_0^2 - E^2) \times \ln U) = n\Sigma(\ln U)^2 + \ln B\ \Sigma \ln U, \tag{4.5}$$

where q is the number of sample spaces. The above two equations are the system of linear equations in two variables which can be solved directly and the constants B and n can be calculated. When solving the equations using Table 4.1, the constants B and n are estimated as 0.512 and 0.299, respectively. So the calibration equation is given by

$$E^2 = 1.188 - 0.512 \cdot U^{0.299}. \tag{4.6}$$

Table 4.2: The difference of calibrated voltage from measured voltage for filament of the bulb.

Measured E^2	Calculated E^2	Error	Error^2
0.708	0.635	0.073	5.34×10^{-3}
0.571	0.575	-0.003	1.14×10^{-5}
0.474	0.536	-0.062	3.88×10^{-3}
0.435	0.508	-0.073	5.33×10^{-3}
0.411	0.465	-0.055	2.99×10^{-3}
0.426	0.420	0.006	3.68×10^{-5}
0.386	0.386	-0.001	3.58×10^{-7}
0.355	0.368	-0.013	1.66×10^{-4}
0.412	0.343	0.068	4.68×10^{-3}
0.359	0.329	0.029	8.57×10^{-4}
0.315	0.299	0.016	2.58×10^{-4}

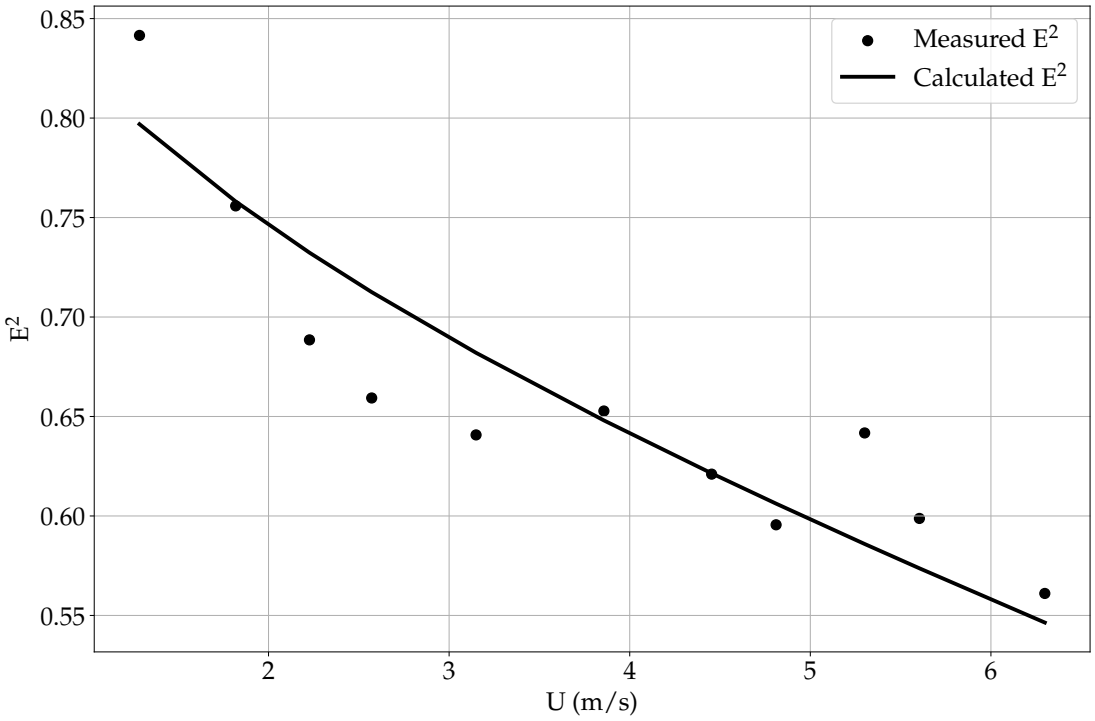

Figure 4.3: Comparison of measured voltage and Calculated voltage of the filament of a bulb.

The velocity of the flow is substituted back in Eq. (4.6) and the voltage is calculated. The error between the measured and calculated voltages is estimated and is given

in Table 4.2. The comparison between the measured and calculated voltages is given in Fig. 4.3. It can be seen that the voltage decreases with an increase in the velocity. When current is supplied to the wire, it will heat up. Due to the increase in heat, the resistance of the wire increases. Now when air flows across the wire, it is cooled by convection and thus its resistance also decreases. So, to maintain the same current on the wire, the voltage across the wire decreases.

The standard deviation σ can be calculated using the equation

$$\sigma = \sqrt{\frac{\Sigma Error^2}{q}} = 0.0463 \qquad \text{and} \qquad 3\sigma = 0.1388 \tag{4.7}$$

The calibration equation for the tungsten filament of the bulb is given by

$$E^2 = 1.188 - 0.512 \cdot U^{0.299} \pm 0.1388 \tag{4.8}$$

4.2 TIME CONSTANT OF THE FILAMENT OF THE BULB

The time constant τ of a sensor is the time taken to produce a steady output when a step input is given to it. The suction fan is kept at a known speed. The bulb filament

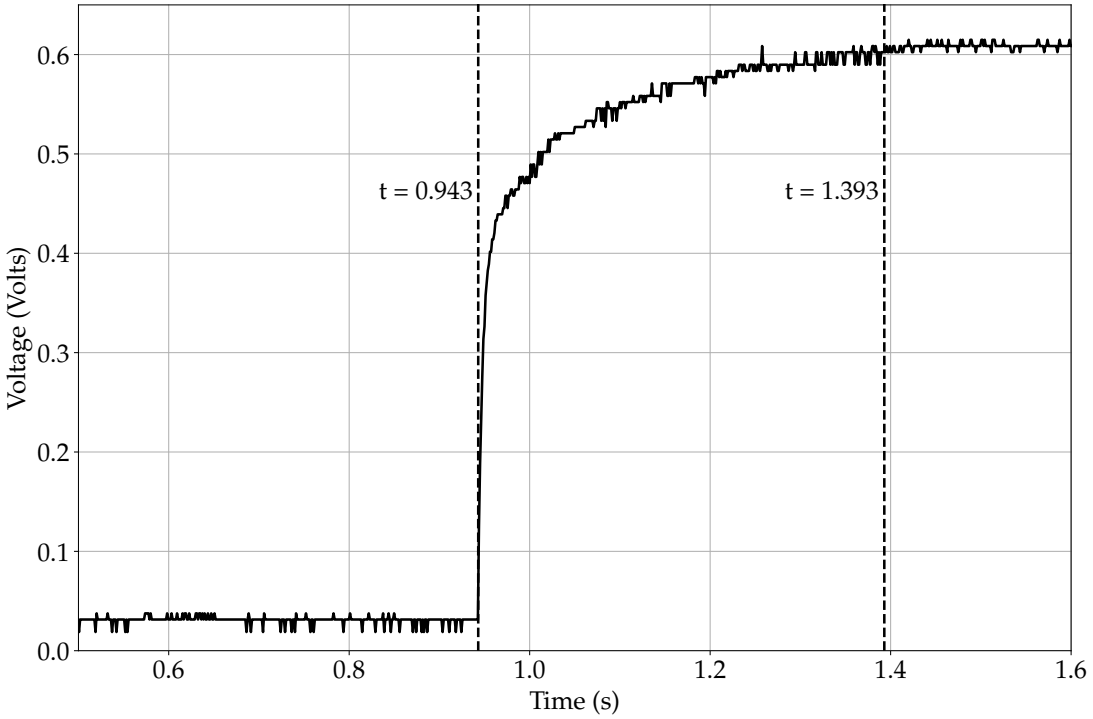

Figure 4.4: Response of the tungsten filament of the bulb to the step input.

is kept inside the test section. The output voltage is then recorded in the oscilloscope. The input constant current is supplied instantaneously to the filament. The sudden

increase in the voltage is also recorded in the oscilloscope. The time taken to reach the maximum steady voltage from the minimum is called the time constant. Figure 4.4 shows the variation of the output voltage with time when input is given instantaneously to the filament. It can be seen from Fig. 4.4 that the filament approximately takes about 450 ms to give steady output when a step input is applied.

4.3 CALIBRATION OF HOT WIRE ANEMOMETER

In this section, the calibration of the hot wire anemometer is discussed. The calibration procedure is the same as that followed in calibration of the tungsten filament of the bulb. The hot wire anemometer is kept at the middle of the wind tunnel and a constant current of 0.1 A is supplied (see Fig. 4.5). Since the diameter of the hot wire is 10 µ the current input is restricted to 0.1 A, which avoids the red hot condition of the hot wire and also oxidation. The output of the hot wire anemometer is recorded for 5 s without any flow which gives the no flow voltage. Further, the speed of the suction fan is slowly increased, and the corresponding output voltage is measured. The hot wire anemometer output voltage is recorded for a pitot tube pressure of 1 Pa, 2 Pa, 3 Pa, 4 Pa, 6 Pa, 9 Pa. The flow velocity can be calculated using Eq. (4.1). The differential pressure, velocity and corresponding voltage output of the filament is given in Table 4.3.

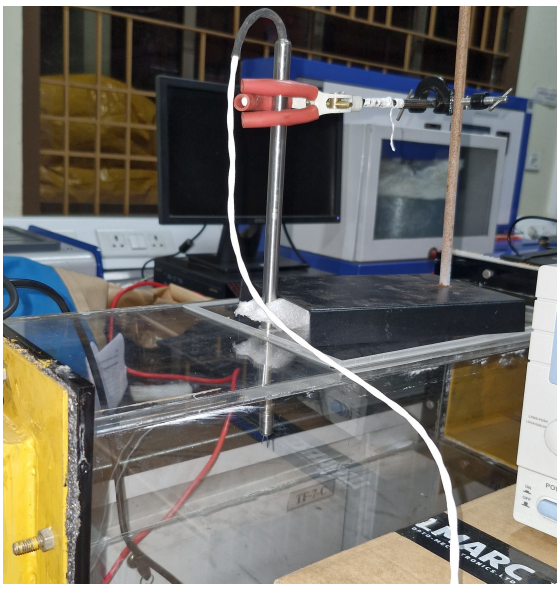

Figure 4.5: Calibration of hot wire anemometer.

The hot wire anemometer is also calibrated using King's law (Eq. (4.2)) and the numerical constants are estimated by the numerical method (method of least squares)

$$E_0 = 1.316\ V$$

Table 4.3: The flow velocity and the output mean voltage of the hot wire anemometer.

Differential Pressure ΔP (Pa)	**Velocity U (m/s)**	**Mean Voltage E (Volts)**
1	1.307	1.002
2	1.849	0.990
3	2.265	0.957
4	2.615	0.933
6	3.203	0.917
9	3.922	0.903

using Eq. (4.4) and Eq. (4.5). On solving the equations, the numerical constants B and n are derived as 0.676 and 0.232, respectively. The calibration equation can be written as

$$E^2 = 1.73 - 0.676 \cdot U^{0.232} \tag{4.9}$$

Equation 4.9 is used to calculate the voltage for different velocities and the error between measured and calculated voltage is given in Table 4.4.

Table 4.4: The difference of calibrated voltage from measured voltage for hot wire anemometer.

Measured E^2	Calculated E^2	Error	Error^2
1.004	1.013	0.009	$8.70\times\ 10^{-5}$
0.981	0.953	0.027	$7.45\times\ 10^{-5}$
0.917	0.916	0.001	$3.72\times\ 10^{-5}$
0.870	0.888	-0.018	$3.34\times\ 10^{-4}$
0.841	0.848	-0.007	$4.84\times\ 10^{-5}$
0.815	0.805	0.010	$9.2\times\ 10^{-5}$

The comparison of the variation of the measured voltage and the calculated voltage with the velocity is given in Fig. 4.6

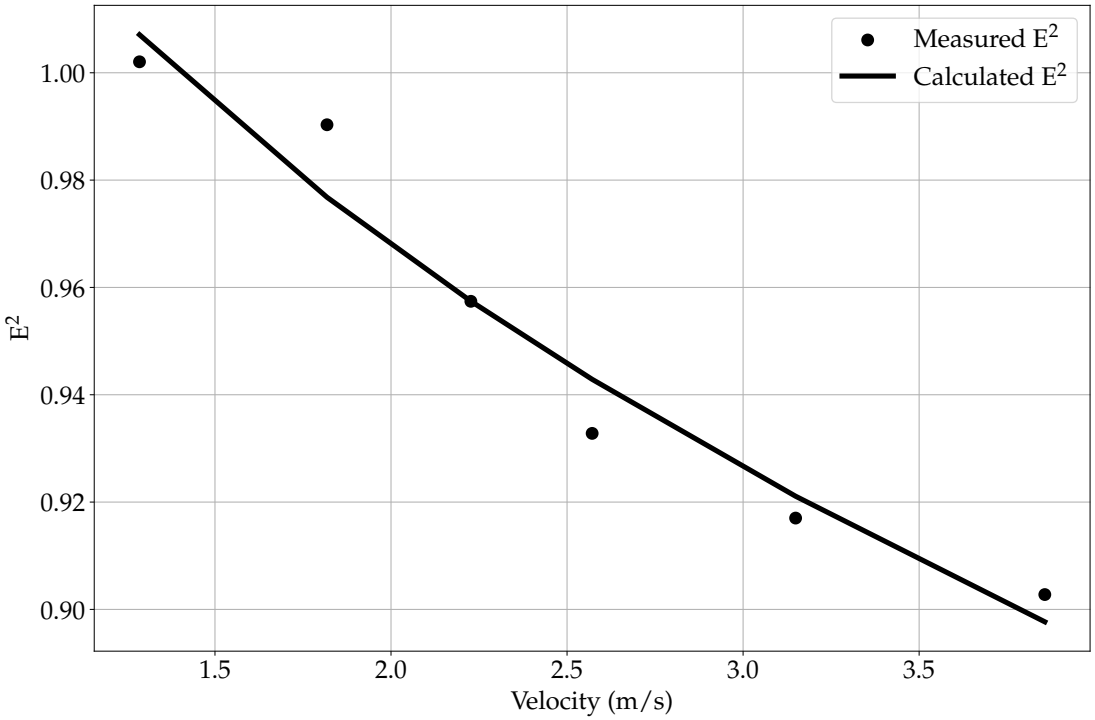

Figure 4.6: Comparison of measured and calculated voltage of the hot wire anemometer

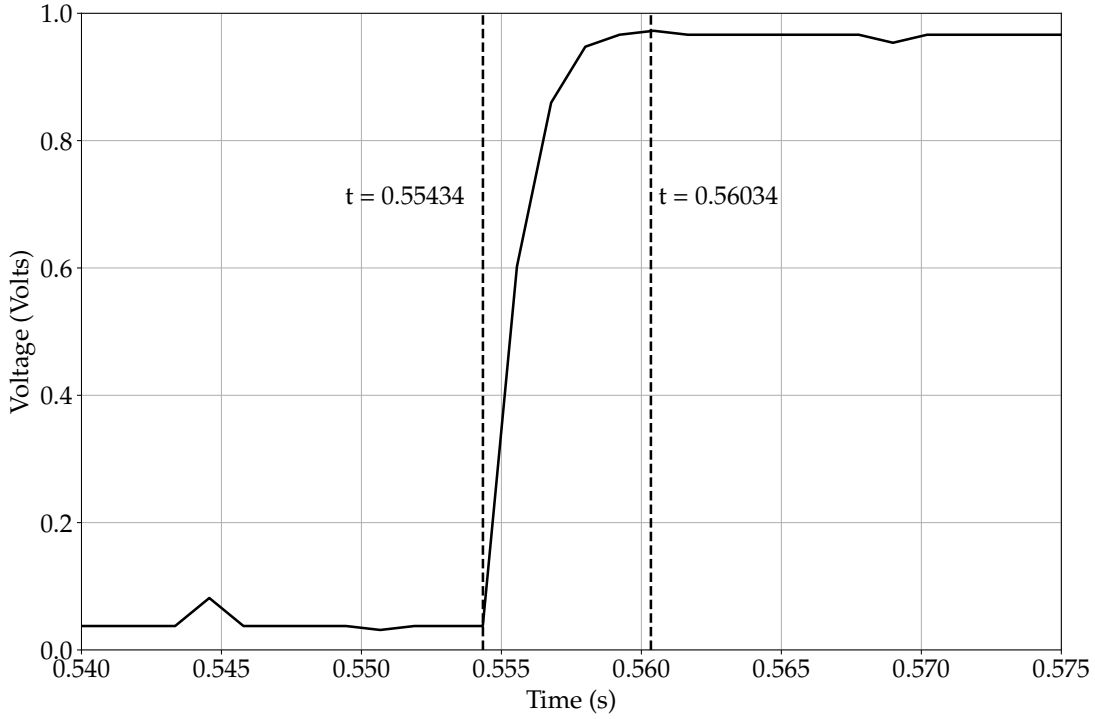

Figure 4.7: Response of a hot wire anemometer for a step input.

4.4 TIME CONSTANT OF THE HOT WIRE ANEMOMETER

The time constant τ of the hot wire anemometer is also estimated by providing a step input to it and recording the output in the oscilloscope. Fig. 4.7 shows the variation of output voltage with time when a step input is given to the anemometer. It can be seen that the hot wire anemometer takes about 6 ms to give steady output.

4.5 CHAPTER SUMMARY

In this chapter, the calibration of the bulb filament and the hot-wire anemometer are discussed. The estimation of time constant is also discussed. It is observed that the time constant of the hot wire anemometer is much (75 times) less than the filament of the bulb. So, it can be concluded that for further analysis in the wind tunnel, the hot wire anemometer is better than the bulb filament. In the next chapter, the vortex analysis in the wind tunnel performed using the hot wire anemometer is discussed.

5

RESULTS AND DISCUSSIONS

In this chapter, the vortex analysis of air flow over a solid cylinder using a constant-current hot wire anemometer is discussed. The vortex analysis is performed at a distance of D, 2 D and 4 D from the cylinder, where D is the diameter of the cylinder. The analysis is also performed at a distance of 0.5 D above the cylinder at all the points mentioned above. The air flow is kept at a pitot tube pressure of 1 Pa, 2 Pa, 3 Pa and 4 Pa. The results are discussed in the following sections.

5.1 VORTEX ANALYSIS AT DISTANCE $x = D$ FROM THE CYLINDER

In this section, the vortex analysis of the flow is done by keeping the hot wire anemometer at a distance of D from the center of the cylinder. Further, the probe is moved to a height of 0.5 D above the center of the cylinder, and the same analysis is performed.

5.1.1 *Vortex analysis at the center of the cylinder*

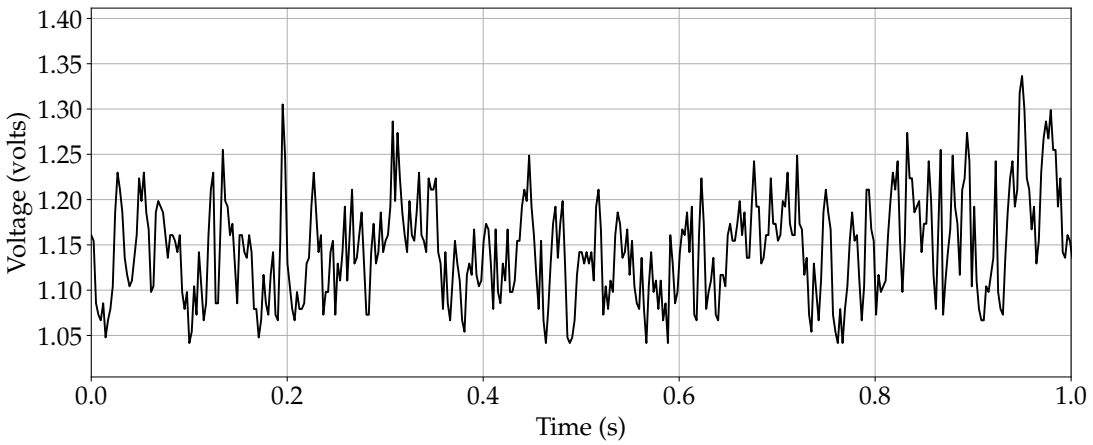

Figure 5.1: The variation of voltage with time for a flow having differential pressure of 1 Pa for sensor placed at a distance of D from the cylinder

The solid cylinder is kept at a distance of 0.20 m from the left end of the test section. The speed of the suction fan is varied from an equivalent differential pressure of 1 Pa, 2 Pa, 3 Pa and 4 Pa using an auto transformer. The output of the hot wire anemometer

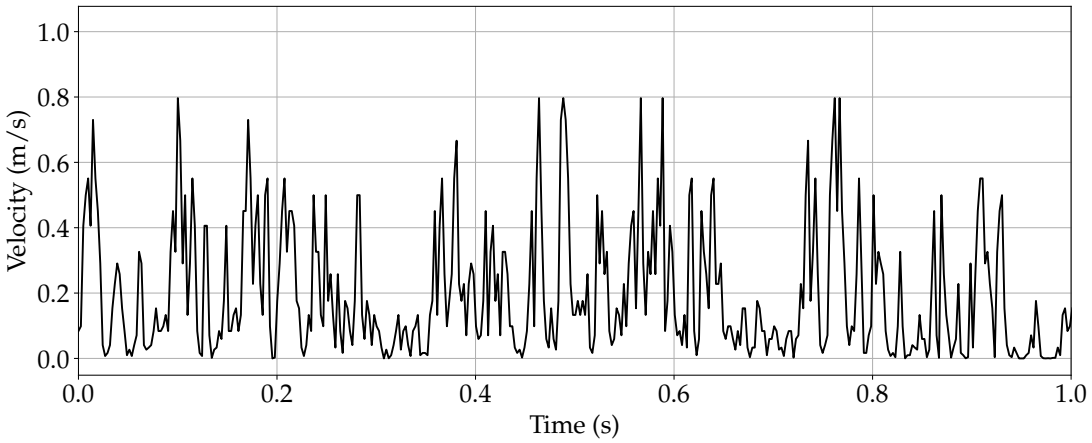

Figure 5.2: The variation of velocity with time for a flow having differential pressure of 1 Pa for sensor placed at a distance of D from the cylinder

is recorded in the PC Oscilloscope for a time of 10 s for all flow pressures. The voltage variation with time for a flow having differential pressure of 1 Pa (between 0 to 1 s) is shown in Fig. 5.1.

The interest is to find the velocity fluctuation in the test section due to the presence of a solid cylinder. The voltage output from the oscilloscope is converted to velocity using the calibration equation (see Eq. (4.9)). The corresponding velocity fluctuation with time is shown in Fig. 5.2.

The fluctuation in flow velocity is due to the occurrence of vortices when the flow is obstructed by the solid cylinder. Here, since the velocity varies with time, it can be assumed to be a function of time. That is,

$$v = v(t). \tag{5.1}$$

Further, the frequency of the vortex can be found by transforming the velocity from temporal domain (t) to frequency domain (ω) using the Fourier transform pairs given by

$$\hat{V}(\omega) = \frac{1}{2\pi}\int_{-\infty}^{\infty} v(t)e^{-i\omega t}dt \tag{5.2}$$

$$v(t) = \int_{-\infty}^{\infty} \hat{V}(\omega)\mathbf{e}^{i\omega t}d\omega \tag{5.3}$$

where $\hat{V}$ is the transformed velocity and ω is the frequency in rad/s ($= 2\pi f$, f - frequency in Hz). The velocity variation is transformed using Eq. 5.2 and resulting frequency variation of velocity spectral density for flow having differential pressure

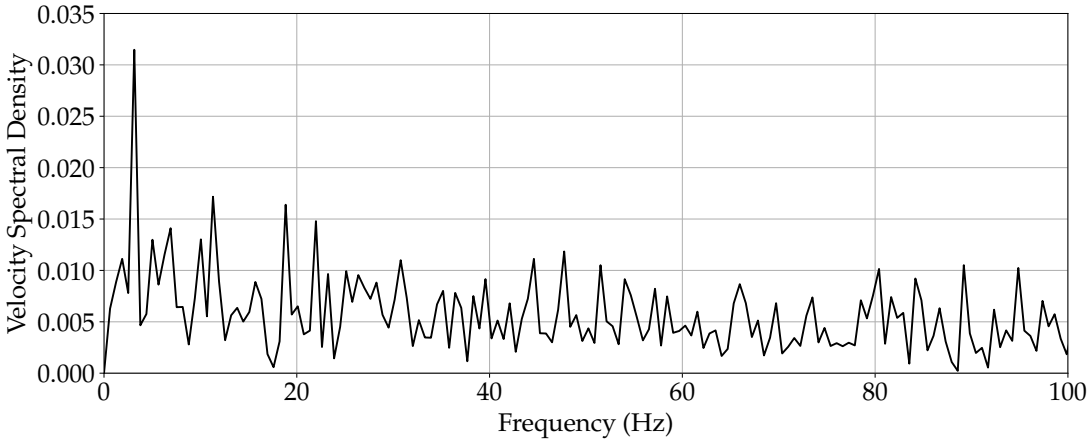

Figure 5.3: Frequency spectrum of velocity.

of 1 Pa (scaled to 0 Hz to 100 Hz) is shown in Fig. 5.3. In this figure, it can be seen that the velocity spectrum peaks at many frequencies. The maximum peak occurs at a frequency of about 3.14 Hz, which corresponds to the frequency of the vortex. Similar frequency peaks are also found in other flow pressures of 2 Pa, 3 Pa and 4 Pa. Eq. (4.1) can be used to find the velocity corresponding to the flow pressure. The Reynolds number for the flow can be calculated using

$$Re = \frac{\rho U D}{\mu}, \tag{5.4}$$

where ρ is the density of air (1.17 kg/m^3), U is the flow velocity in m/s, D is the diameter of the solid cylinder (0.033 m) and μ is the dynamic viscosity of air (1.87×10^{-5} $kg/m \cdot s$). A comparison of velocity spectral density with frequency for all flow velocities (written in terms of Reynolds number) is shown in Fig. 5.4.

It can be seen in Fig. 5.4 that at each flow velocity, the peak frequency is different. This is due to the difference in the formation of the vortex at each velocity. At Reynolds numbers 2699 and 4676, the maximum peak occurs at a frequency of 3.14 Hz and at Reynolds numbers 3818 and 5399, the peak is at 2.51 Hz. The Reynolds number is the ratio of inertial forces to viscous forces. It describes whether the flow is laminar or turbulent. Similarly, the Strouhal number (St) is the ratio of oscillatory inertial forces to steady inertial force. It describes the relationship between an unsteady phenomenon (vortex shedding) and flow velocity. The Strouhal number is defined as

$$St = \frac{f \cdot D}{U}, \tag{5.5}$$

where f is the frequency of the vortex in Hz, D is the diameter of the solid cylinder and U is the flow velocity. Assuming that the peak frequency in Fig. 5.4 dominates the entire spectrum, the peak frequency for all flows is used to calculate the Strouhal

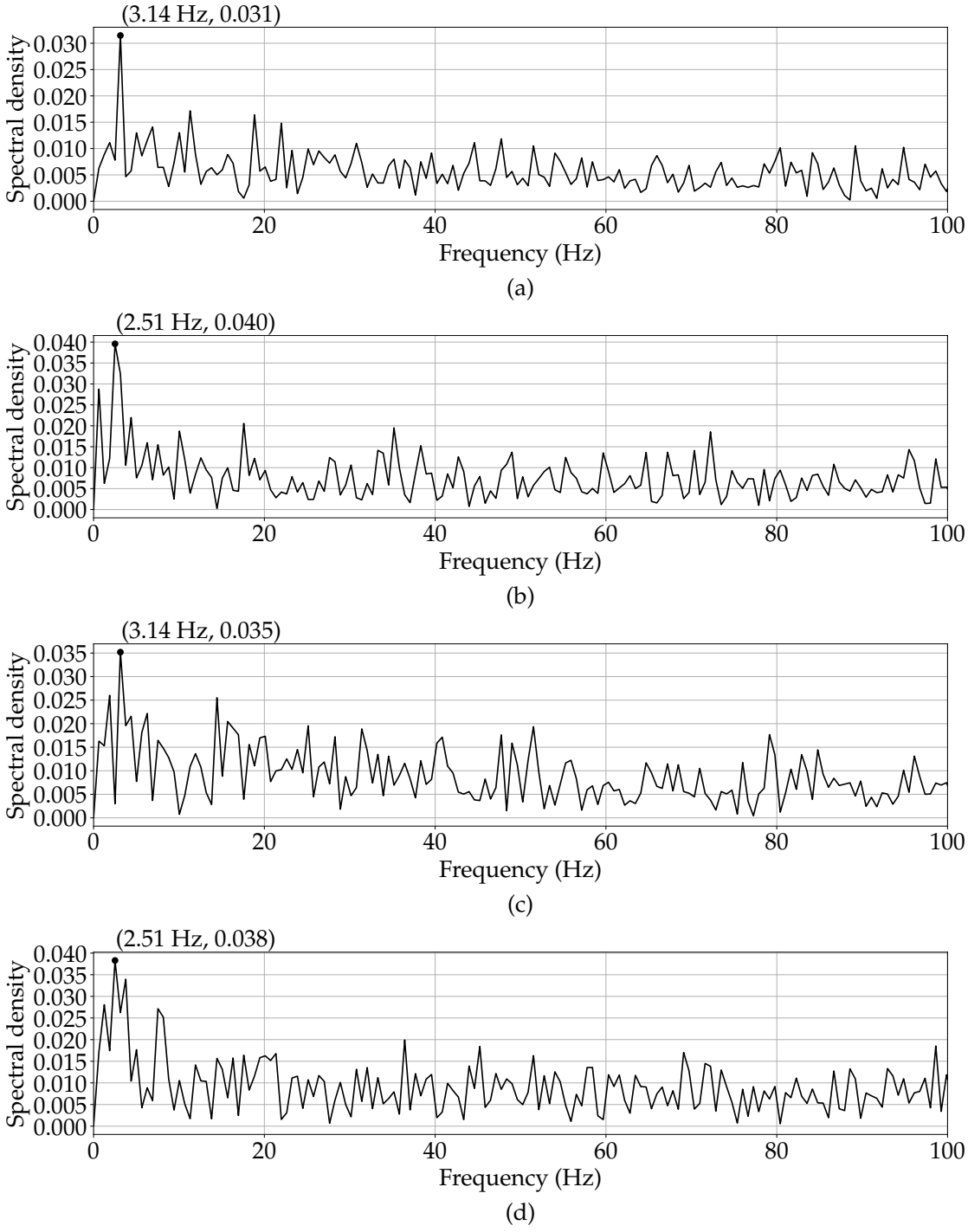

Figure 5.4: Frequency spectral density of velocity for flow Reynolds number (a) 2699, (b) 3818, (c) 4676 and (d) 5399 at a distance of D from the center of the cylinder.

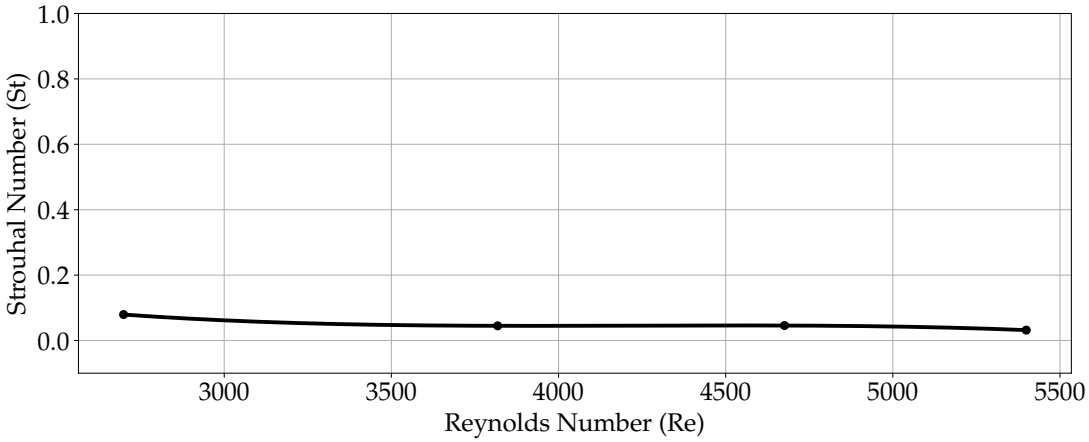

Figure 5.5: Variation of Strouhal number (St) with Reynolds number (Re) for flow past a cylinder at a distance of "D" from the center.

number. The two non-dimensional numbers (Reynolds number and Strouhal number) are plotted against each other in Fig. 5.5. In the figure, it can be seen that the Strouhal number is decreasing slightly with Reynolds number. This is because the frequency of the vortex decreases with an increase in flow velocity. The next section discusses the vortex analysis at a distance of D and a height of 0.5 D from the center of the cylinder.

5.1.2 *Vortex analysis at a height of* 0.5 D *from the center of the cylinder*

The hot wire anemometer is moved to a height of 0.5 D from the center of the cylinder and analysis is performed for four flow speeds having differential pressure of 1 Pa, 2 Pa, 3 Pa and 4 Pa. Here, for each flow velocity, the voltage output is measured in the oscilloscope. The corresponding velocity is calculated from the calibration equation (Eq. (4.9)). The velocity is then transformed from the temporal domain to the frequency domain using the Fourier transform equation (Eq. (5.2)). A comparison of velocity spectral density with frequency for all flow velocities is shown in Fig. 5.6. In the figure, it can be seen that the peak frequency for each flow velocity is different from the peak obtained previously. For $Re = 2699$, the peak frequency is 5.65 Hz, for $Re = 3818$, peak frequency is at 37.06 Hz, for $Re = 4676$, the peak frequency is 3.14 Hz and for $Re = 5399$, the peak frequency is 0.63 Hz. These peak frequencies are then used to calculate the Strouhal number (Eq. (5.5)). The Strouhal number variation with Reynolds number is shown in Fig. 5.7. Here, it can be seen that the Strouhal number fluctuates highly in the region of $Re = 3000$ to $Re = 4500$. This indicates a change of vortex shedding characteristics when the flow is in transition toward turbulence. The next

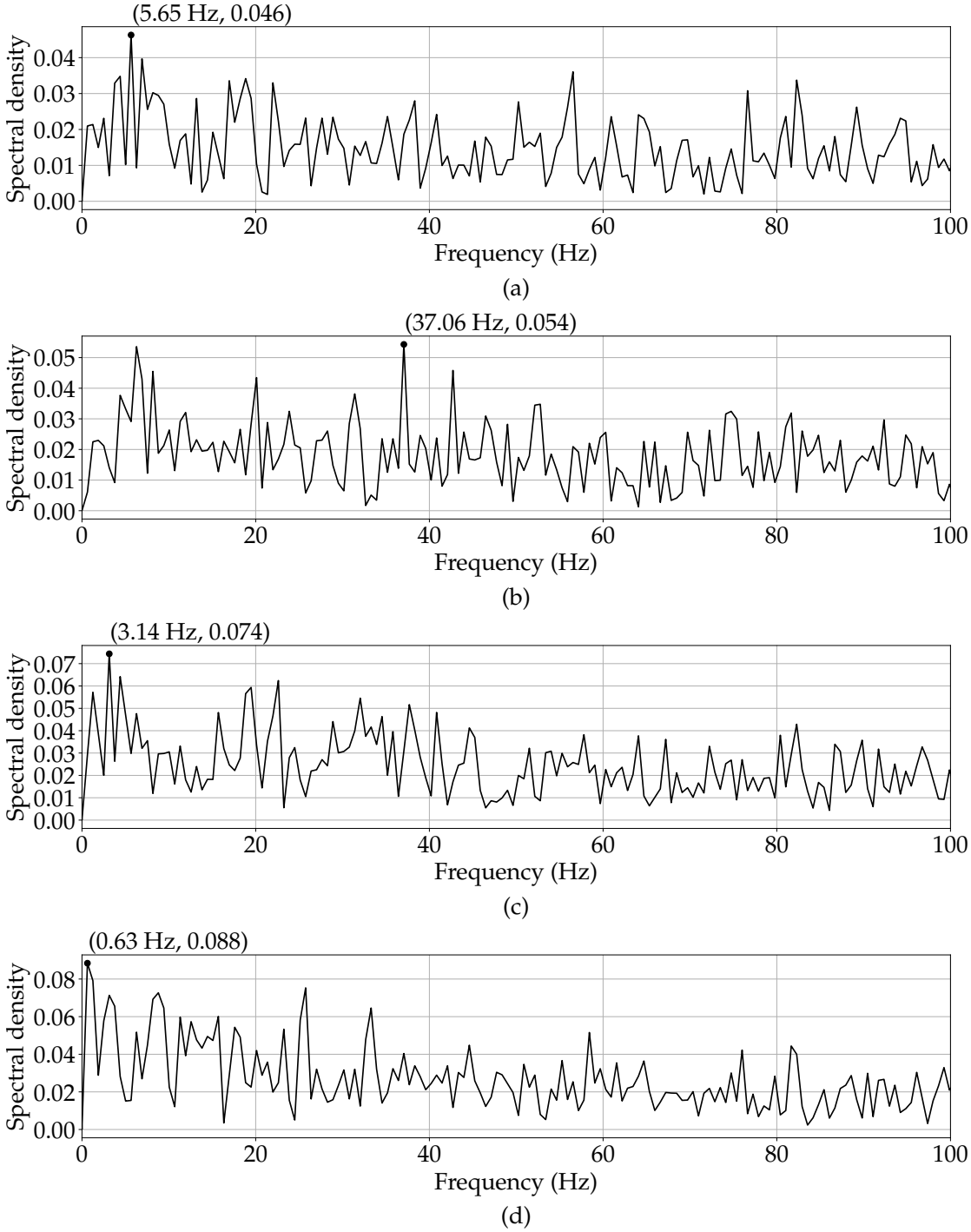

Figure 5.6: Frequency spectral density of velocity for flow Reynolds number (a) 2699, (b) 3818, (c) 4676 and (d) 5399 at a distance of "D" and a height of "0.5 D" from the center of the cylinder.

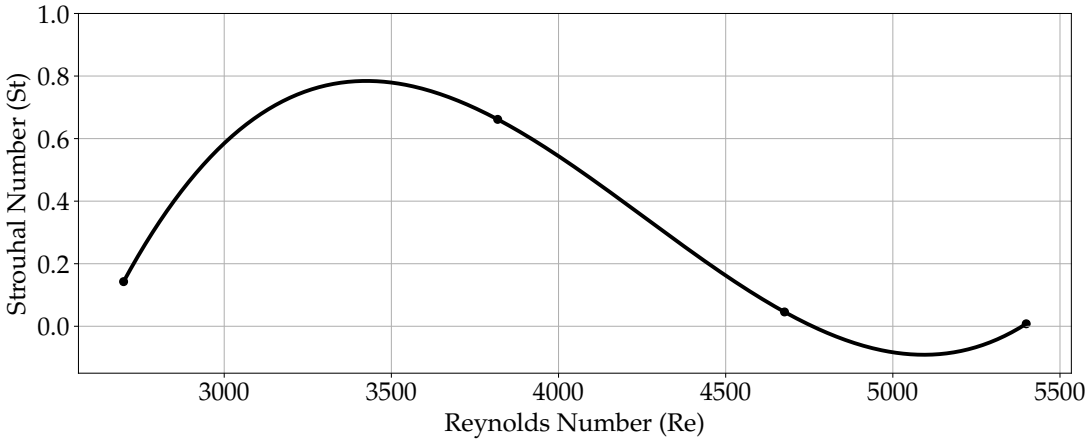

Figure 5.7: Variation of Strouhal number (St) with Reynolds number (Re) for flow past a cylinder at a distance of "D" and at a height of "0.5 D" from the center of the cylinder.

section discusses the vortex shedding characteristics at a distance of 2 D from the center of the cylinder.

5.2 VORTEX ANALYSIS AT DISTANCE x = 2D FROM THE CYLINDER

In this section, the vortex shedding characteristics at a distance of 2 D from the cylinder is discussed. The analysis is carried out at the center of the cylinder and at a height of 0.5 D from the cylinder.

5.2.1 *Vortex analysis at the center of the cylinder*

The hot wire anemometer is kept at a distance of 2 D downstream of the cylinder and the vortices are analyzed for air flow having differential pressures of 1 Pa, 2 Pa, 3 Pa and 4 Pa. The output voltage is measured using an oscilloscope and the corresponding velocity is calculated using the calibration equation (Eq. (4.9)). The velocity is transformed from the temporal domain to the frequency domain using Fourier transform (Eq. (5.2). A comparison of velocity spectral density with frequency for all flow velocities is shown in Fig. 5.8. It can be seen that for $Re = 2699$, the peak frequency is 19.47 Hz, for $Re = 3818$, peak frequency is at 3.77 Hz, for $Re = 4676$, the peak frequency is 0.63 Hz and for $Re = 5399$, the peak frequency is 3.77 Hz. Using these peak frequencies, the Strouhal number is calculated. The variation of the Strouhal number with the Reynolds number is shown in Fig. 5.9.

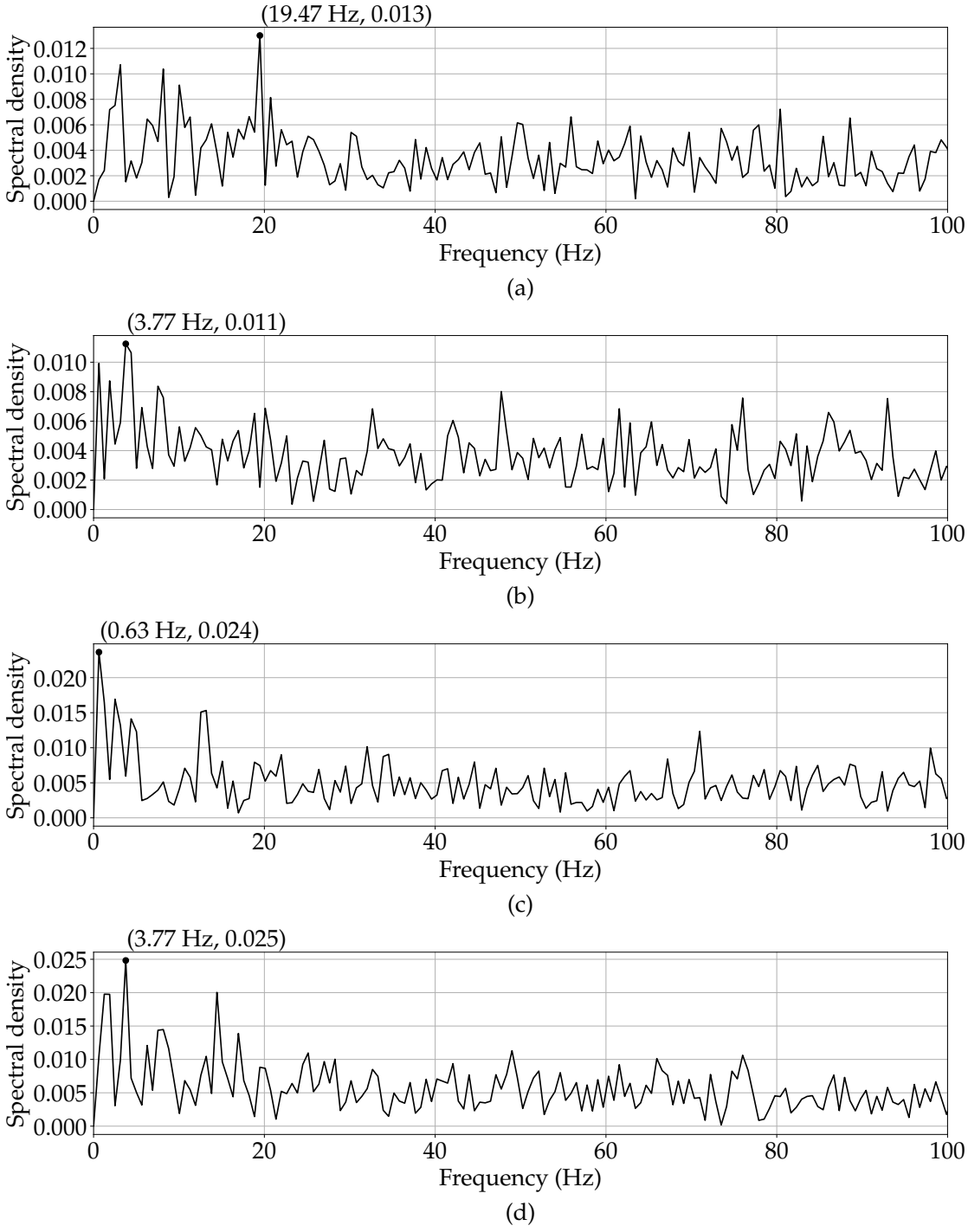

Figure 5.8: Frequency spectral density of velocity for flow Reynolds number (a) 2699, (b) 3818, (c) 4676 and (d) 5399 at a distance of "2 D" from the center of the cylinder.

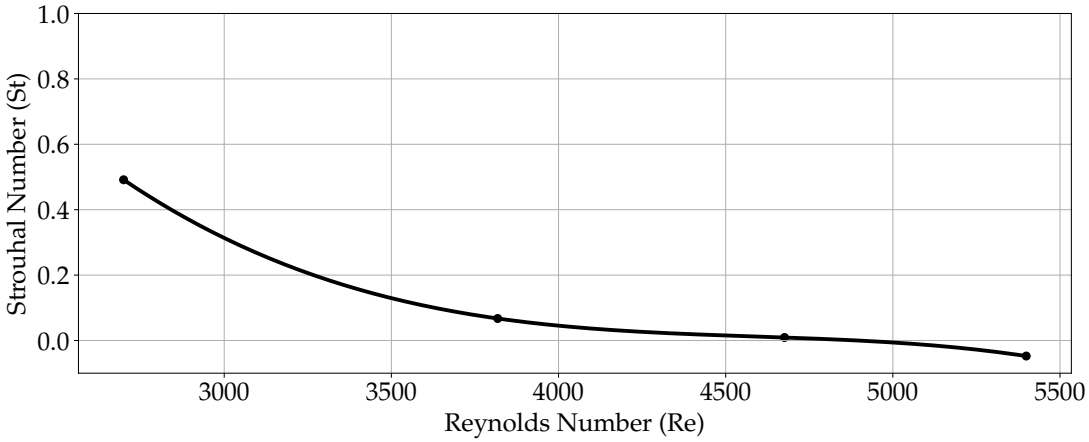

Figure 5.9: Variation of Strouhal number (St) with Reynolds number (Re) for flow past a cylinder at a distance of "2 D" from the center of the cylinder.

In Fig. 5.9, it can be seen that the Strouhal number decreases with an increase in the Reynolds number. This is because of the reduction of the frequency of vortices with increase in velocity.

5.2.2 *Vortex analysis at a height of* 0.5 D *from the center of the cylinder*

The hot wire anemometer is then moved to a height of 0.5 D from the center of the cylinder and the analysis is performed again for the four flow speeds with differential pressures of 1 Pa, 2 Pa, 3 Pa and 4 Pa. For each flow velocity, the voltage output from the hot wire anemometer is measured in the oscilloscope. The velocities corresponding to the voltages are calculated from the calibration equation (Eq. (4.9)). Then it is transformed from the temporal domain to the frequency domain using the Fourier transform equation (Eq. (5.2)). A comparison of velocity spectral density with frequency for all flow velocities is shown in Fig. 5.10.

The peak frequencies are 1.88 Hz for $Re = 2699$, 1.88 Hz for $Re = 3818$, 7.54 Hz for $Re = 4676$ and 10.68 Hz for $Re = 5399$. These peak frequencies are used to calculate the Strouhal number (Eq. (5.5)) and is plotted against the Reynolds number. The comparison between the Reynolds number and the Strouhal number is shown in Fig. 5.11. Here, the Strouhal number increases with an increase in Reynolds number. This is due to the increase of the vortex frequency when there is an increase in the flow speed. The next section discusses the vortex shedding characteristics at a distance of 4 D from the center of the cylinder.

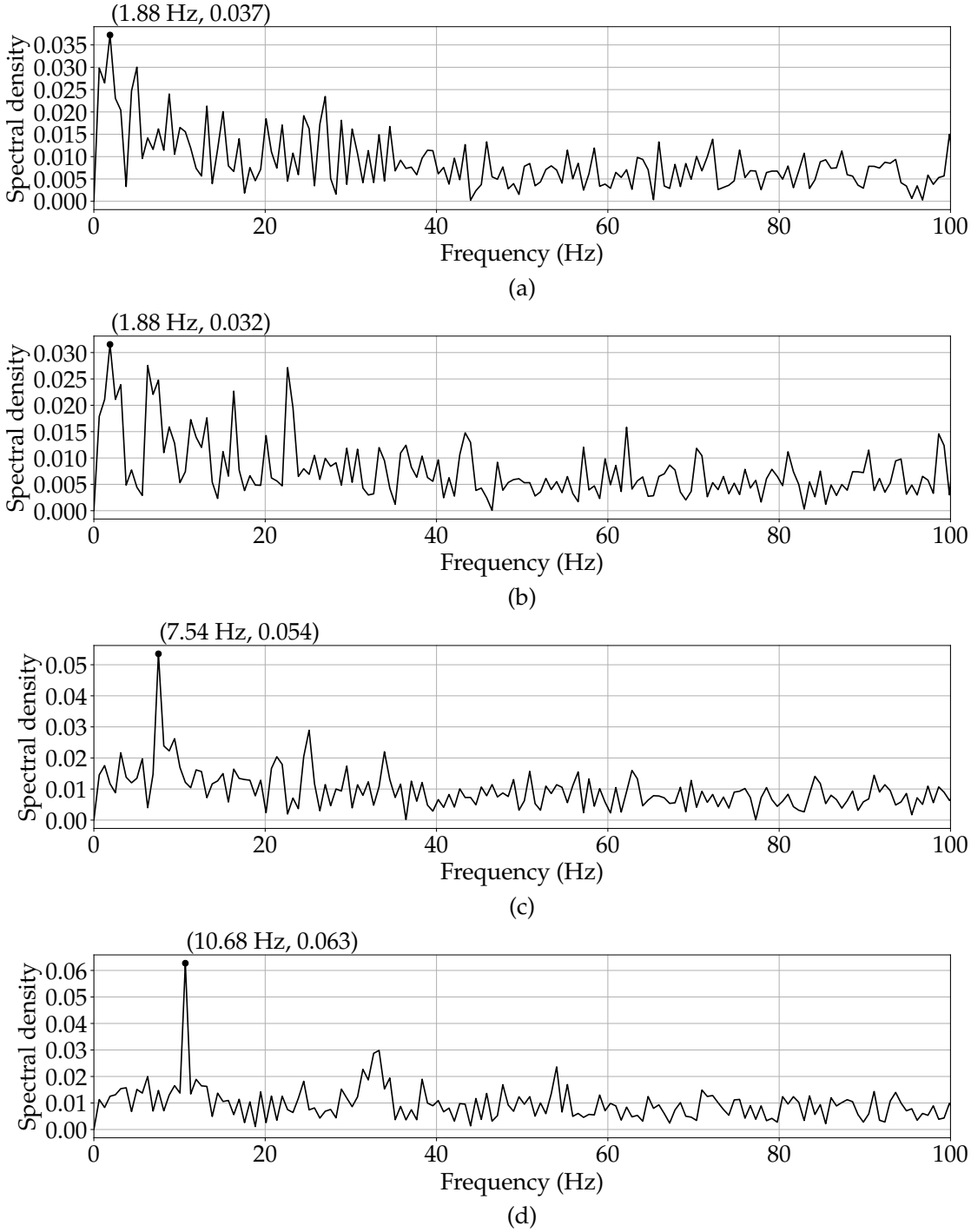

Figure 5.10: Frequency spectral density of velocity for flow Reynolds number (a) 2699, (b) 3818, (c) 4676 and (d) 5399 at a distance of "2 D" and a height of "0.5 D" from the center of the cylinder.

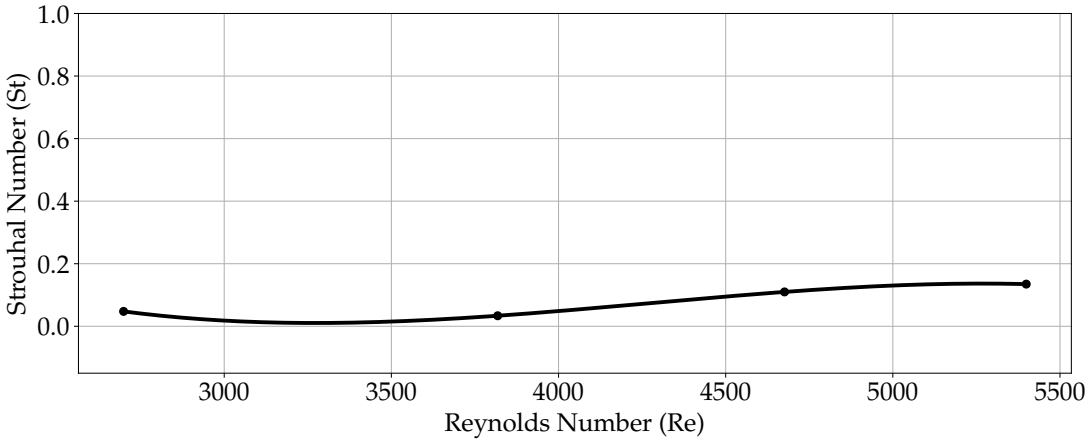

Figure 5.11: Variation of Strouhal number (St) with Reynolds number (Re) for flow past a cylinder at a distance of "2 D" and at a height of "0.5 D" from the center of the cylinder.

5.3 VORTEX ANALYSIS AT DISTANCE x = 4D FROM THE CYLINDER

In this section, the vortex analysis is performed at a distance of 4 D from the cylinder. The analysis is carried out at the center of the cylinder and at a height of 0.5 D from the cylinder.

5.3.1 *Vortex analysis at the center of the cylinder*

The hot wire anemometer is kept at a distance of 4 D downstream of the cylinder and vortex analysis is carried out for air flow having differential pressures of 1 Pa, 2 Pa, 3 Pa and 4 Pa. The output voltage across the hot wire anemometer is measured using an oscilloscope and the corresponding velocity is calculated using the calibration equation (Eq. (4.9)). The velocity is transformed from the temporal domain to the frequency domain using Fourier transform (Eq. (5.2). A comparison of velocity spectral density with frequency for all flow velocities is shown in Fig. 5.12. It can be seen that for Re = 2699, the peak frequency is 5.65 Hz, for Re = 3818, peak frequency is at 1.26 Hz, for Re = 4676, the peak frequency is 5.65 Hz and for Re = 5399, the peak frequency is 0.63 Hz. Using these peak frequencies, the Strouhal number is calculated. The variation of the Strouhal number with the Reynolds number is shown in Fig. 5.13. The Strouhal number is in the range 0 to 0.2 which is normal but the low fluctuation is due to its transition towards turbulence.

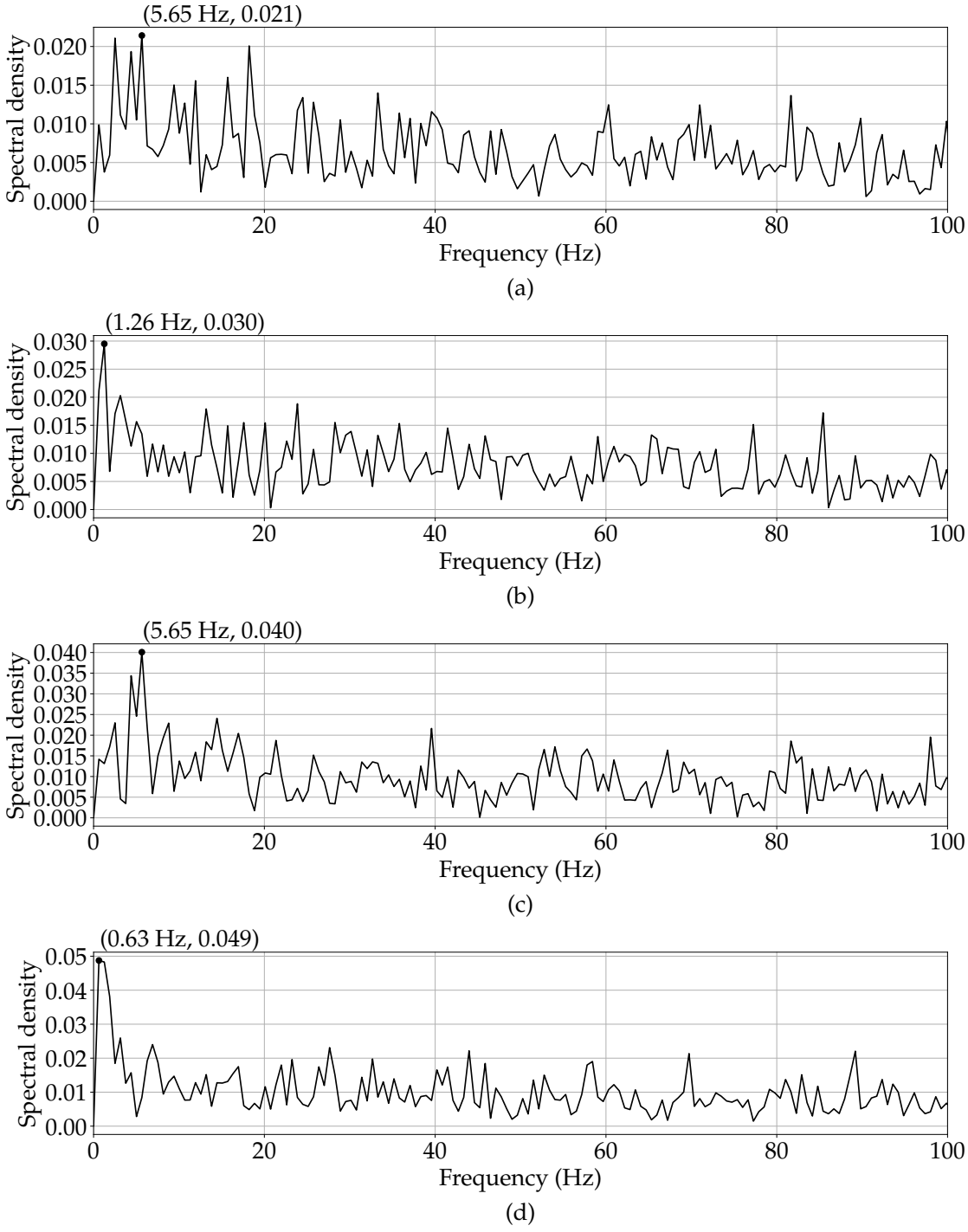

Figure 5.12: Frequency spectral density of velocity for flow Reynolds number (a) 2699, (b) 3818, (c) 4676 and (d) 5399 at a distance of "4 D" from the center of the cylinder.

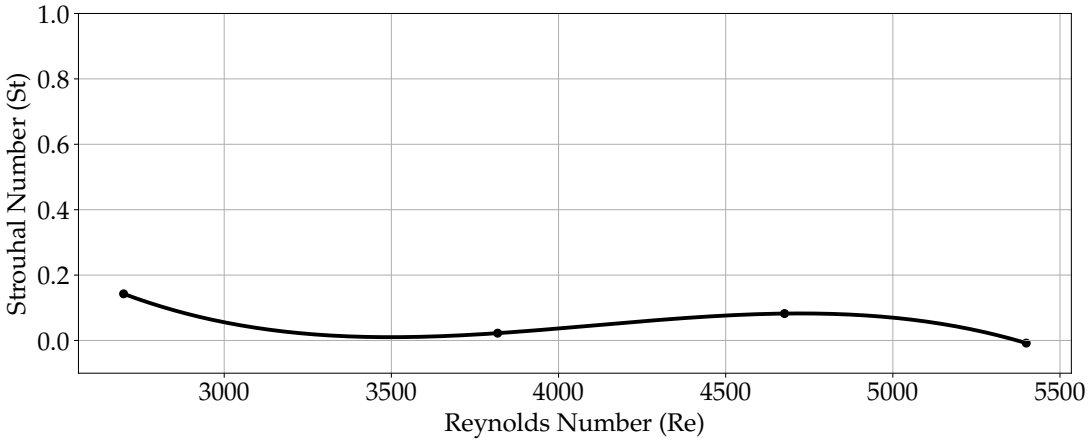

Figure 5.13: Variation of Strouhal number (St) with Reynolds number (Re) for flow past a cylinder at a distance of "4 D" from the center of the cylinder.

5.3.2 *Vortex analysis at a height of* 0.5 D *from the center of the cylinder*

The hot wire anemometer is shifted to a height of 0.5 D from the center of the cylinder and vortex analysis is performed for all tow speeds. The voltage output is measured across the sensor in the oscilloscope. The corresponding velocity is calculated from the calibration equation (Eq. (4.9)). The velocity is then transformed from the temporal domain to the frequency domain using the Fourier transform equation (Eq. (5.2)). A comparison of velocity spectral density with frequency for all flow velocities is shown in Fig. 5.14. It can be seen in Fig. 5.14 that the peak frequencies are 1.26 Hz for $Re = 2699$, 1.26 Hz for $Re = 3818$, 1025.79 Hz for $Re = 4676$ and 1282.71 Hz for $Re = 5399$. The high increase in frequency is due to increased disturbances as the flow is in transition to turbulence. These peak frequencies are used to calculate the Strouhal number (Eq. (5.5)) and is plotted against the Reynolds number. The comparison between the Reynolds number and the Strouhal number is shown in Fig. 5.15.

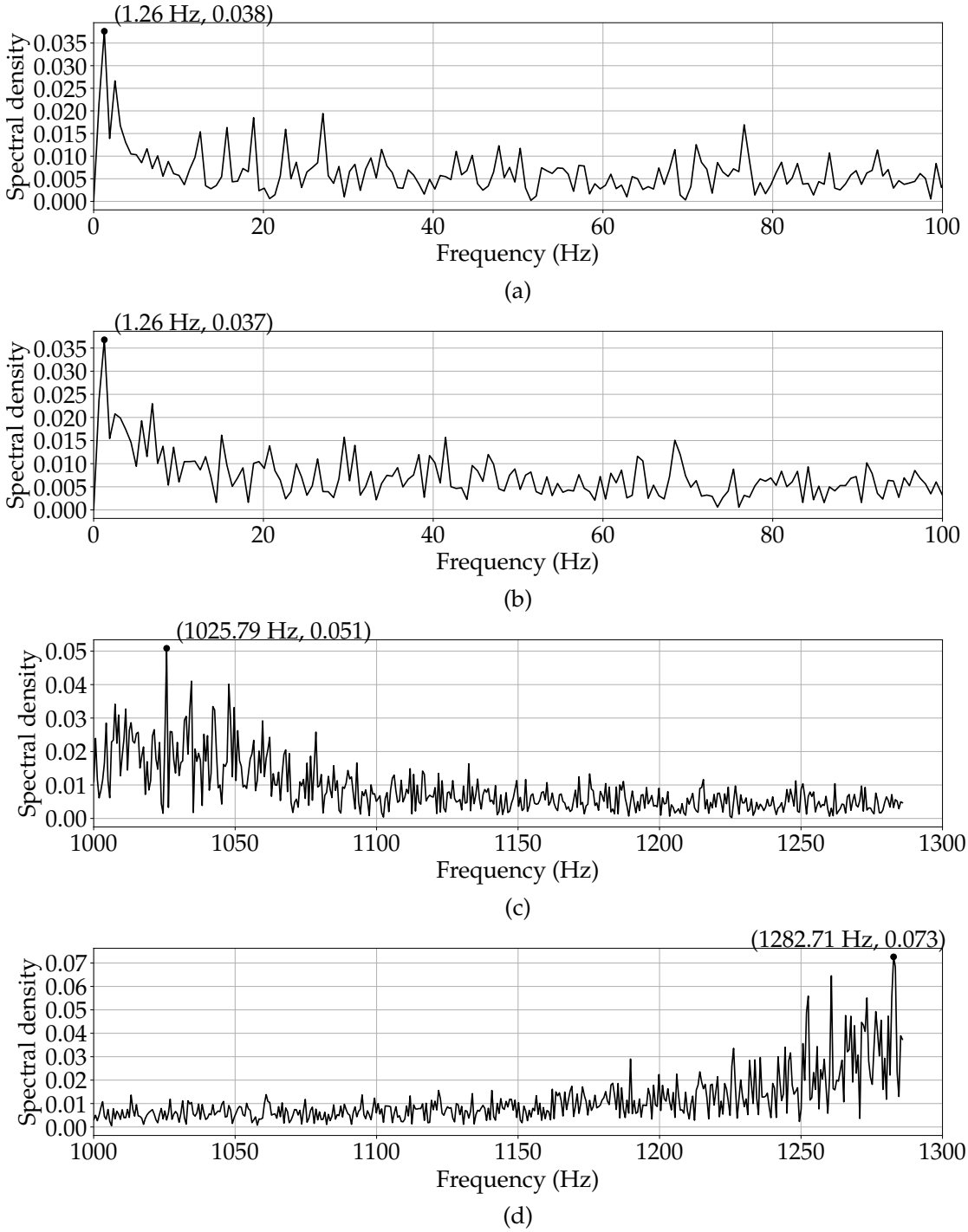

Figure 5.14: Frequency spectral density of velocity for flow Reynolds number (a) 2699, (b) 3818, (c) 4676 and (d) 5399 at a distance of "4 D" and a height of "0.5 D" from the center of the cylinder.

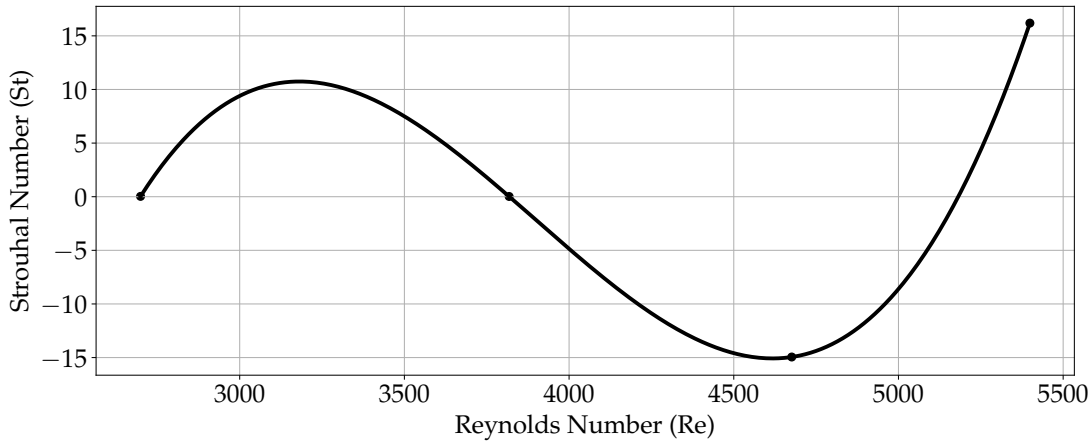

Figure 5.15: Variation of Strouhal number (St) with Reynolds number (Re) for flow past a cylinder at a distance of "4 D" and a height of "0.5 D" from the center of the cylinder.

5.4 CHAPTER SUMMARY

In this chapter, the vortex shedding analysis for a flow with differential pressures of 1 Pa, 2 Pa, 3 Pa and 4 Pa is discussed. For this analysis, a hot wire anemometer calibrated using a pitot static tube is used. The vortex shedding behavior is studied at various locations in the test section of the wind tunnel. The solid cylinder with diameter $D = 0.033$ m is placed at a distance of 0.2 m from the left end of the test section. The hot wire anemometer is placed at a distance of D, 2 D and 4 D from the center of the cylinder and at a height of 0.5 D from each location. The voltage variation of the sensor is measured and its corresponding velocity variation is calculated using the calibration equation (Eq. (4.9)) in temporal domain. Then it is converted to the frequency domain using the forward Fourier transform equation (Eq. (5.2)). The peak frequency of the vortex is calculated at each point and the corresponding Strouhal number (Eq. (5.5)) is calculated. The variation of Strouhal number is plotted with Reynolds number at all six locations. The Strouhal number is found to vary between 0 and 0.2 in some locations, and it is deviating very largely at other locations. This is due to the flow transition from laminar region to turbulence.

Part III

CONCLUSION AND FUTURE SCOPE

6

CONCLUSIONS

This project successfully investigated vortex shedding around a cylindrical body using a custom designed and fabricated wind tunnel under controlled airflow conditions. By analyzing Reynolds numbers (Re) in the range of 2699 to 5399 and the corresponding Strouhal numbers (St) between 0.2 and 0.6, the study established the relationship between flow velocity and vortex shedding characteristics. The peak vortex shedding frequencies ranged from 0.63 Hz to 37.06 Hz across different flow velocities and measurement locations, highlighting the dynamic nature of flow interactions with the solid cylinder.

A significant outcome of the project is the successful calibration and implementation of a custom-built hot wire anemometer, with constants B = 0.676 and n = 0.232 (in King's law), for precise airflow velocity measurements. The hot wire anemometer achieved a time constant of 6 ms, significantly faster compared to the tungsten filament sensor, which had a time constant of 450 ms. This considerable difference underscores the superior responsiveness of the hot-wire anemometer to capture rapid flow fluctuations. Additionally, smoke visualization vividly illustrated the formation and shedding of vortices behind the cylinder, complementing the quantitative measurements.

The results showed a clear trend in vortex shedding behavior, with Strouhal numbers decreasing slightly as Reynolds numbers increased, indicating a lower vortex frequency at higher velocities. This trend was most evident in regions of transitioning turbulence, offering valuable insights into the interplay between inertial and viscous forces in fluid flow. The study also revealed variations in the vortex shedding frequencies at different measurement heights from the center of the solid cylinder, emphasizing the spatial complexity of flow dynamics.

The findings enhance the understanding of fluid dynamics, particularly the relationship between flow velocity, vortex frequency, and turbulence. This research provides a solid foundation for future studies in advanced sensing techniques, computational fluid dynamics simulations, and structural designs that address vortex-induced vibrations. It highlights the importance of combining experimental and theoretical approaches to advance research in fluid mechanics.

6.1 FUTURE SCOPE

Testing different geometries or adding varying surface roughness to cylindrical objects in future studies, combined with advanced sensing techniques, could help identify how vortex shedding behaviors change under different physical conditions.

Piezoelectric and piezoresistive sensors can be used for more comprehensive flow and pressure measurements. Piezoelectric sensors can capture dynamic pressure fluctuations, while piezoresistive sensors can offer more stable, continuous measurements of strain and pressure, providing a broader range of data for vortex analysis. The data gathered from both piezoelectric and piezoresistive sensors could be compared with computational fluid dynamics (CFD) simulations for validation, helping to refine the experimental results and improve the understanding of vortex shedding and flow characteristics at various Reynolds numbers.

The hot wire anemometer can be improved by integrating modern data acquisition systems with higher sampling rates and reduced noise interference. Additionally, laser-based techniques such as Particle Image Velocimetry (PIV) could provide more detailed velocity field visualizations.Scaled-down models of industrial and natural structures can be tested in the wind tunnel to simulate real-world scenarios. This approach can help optimize designs and improve the resilience of structures subjected to vortex-induced forces.

Insights from vortex shedding studies can be applied to the design of efficient energy systems, such as wind turbines and vortex-induced energy harvesters. Further, studying pollutant dispersion in wakes could have implications for environmental modeling and management. Extending the research to higher Reynolds numbers could uncover nonlinear flow behaviors and transitional phenomena, providing a deeper understanding of turbulence and wake dynamics in fluid systems.

BIBLIOGRAPHY

[1] C.J. Doolan, V. Choley, and J. Crespel. "Vortex shedding during the interaction of a turbulent wake with a cylinder." In: *Journal of Fluids and Structures* 31 (2012), pp. 141–146. ISSN: 0889-9746. DOI: https://doi.org/10.1016/j.jfluidstructs.2012.02.010. URL: https://www.sciencedirect.com/science/article/pii/S0889974612000527.

[2] U Hartmann. "Wall interference effects on hot-wire probes in a nominally two-dimensional highly curved wall jet." In: *Journal of Physics E: Scientific Instruments* 15.7 (July 1982), p. 725. DOI: 10.1088/0022-3735/15/7/009. URL: https://dx.doi.org/10.1088/0022-3735/15/7/009.

[3] N. Hosseini, M.D. Griffith, and J.S. Leontini. "The flow past large numbers of cylinders in tandem." In: *Journal of Fluids and Structures* 98 (2020), p. 103103. ISSN: 0889-9746. DOI: https://doi.org/10.1016/j.jfluidstructs.2020.103103. URL: https://www.sciencedirect.com/science/article/pii/S0889974619309843.

[4] Ishan J Kelkar, Shreekumar S Kamalapurkar, and Ketan V Karandikar. "Design, Fabrication and Testing of Low-Subsonic Open-Circuit Wind Tunnels-A Review." In: *International Journal of Engineering Research & Technology (IJERT)* 8.10 (2019).

[5] Amol L Mangrulkar, Shubham Bagade, Saurabh Chavan, Jiteshkumar Babani, and Shreepad Bhagat. "Design and fabrication of an open circuit subsonic wind tunnel for educational purposes." In: *Int Res J Eng Technol (IRJET)* 6.04 (2019), pp. 2395–0056.

[6] Ferid Rehimi and Fethi Aloui. "Synchronized analysis of an unsteady laminar flow downstream of a circular cylinder centred between two parallel walls using PIV and mass transfer probes." In: *Experiments in Fluids* 51 (July 2010), pp. 1–22. DOI: 10.1007/s00348-010-1005-y.

[7] Mehmet Sahin and Robert G. Owens. "On the effects of viscoelasticity on two-dimensional vortex dynamics in the cylinder wake." In: *Journal of Non-Newtonian Fluid Mechanics* 123.2 (2004), pp. 121–139. ISSN: 0377-0257. DOI: https://doi.org/10.1016/j.jnnfm.2004.08.002. URL: https://www.sciencedirect.com/science/article/pii/S0377025704002538.

[8] Sintu Singha and K.P. Sinhamahapatra. "Flow past a circular cylinder between parallel walls at low Reynolds numbers." In: *Ocean Engineering* 37.8 (2010), pp. 757–769. ISSN: 0029-8018. DOI: https://doi.org/10.1016/j.oceaneng.2010.02.012. URL: https://www.sciencedirect.com/science/article/pii/S0029801810000570.